Short-term moderate caloric restriction in the rhesus macaque attenuates markers of ovarian aging in select populations

Emma S. Gargus[1],*, Rhea Sharma[1],*, Rebecca Gu[1], Camille Mulcahy[1], Brian W. Johnson[2], Jing Song[3], Jungwha Lee[3], Mary Zelinski[4,5], Francesca E. Duncan[1]

[1]Department of Obstetrics and Gynecology, Feinberg School of Medicine, Northwestern University, Chicago, IL 60611, USA
[2]Department of Comparative Medicine, Histology and Imaging Core, University of Washington, Seattle, WA 98195, USA
[3]Department of Preventive Medicine, Feinberg School of Medicine, Northwestern University, Chicago, IL 60611, USA
[4]Division of Reproductive and Developmental Sciences, Oregon National Primate Research Center, Beaverton, OR 97006, USA
[5]Department of Obstetrics and Gynecology, Oregon Health and Science University, Portland, OR 97239, USA
*Co-first authors

Correspondence to: Francesca E. Duncan; **email:** f-duncan@northwestern.edu

ABSTRACT

Ovarian aging results in decreased fertility and endocrine function. In mice, caloric restriction (CR) maintains ovarian function. In this study, we determined whether CR also has a beneficial effect on reproductive longevity in the nonhuman primate (NHP). Ovaries were collected from young (10–13 years) and old (19–26 years) rhesus macaques who were either on a diet of moderate caloric restriction or a control diet for three years. To test the effect of CR on follicle number, follicles were analyzed in histological sections from animals across experimental cohorts: Young Control, Young CR, Old Control, Old CR (n = 4–8/group). In control animals, there was an age-dependent decrease in follicle numbers across all follicle stages ($P < 0.05$). Although there was no effect of diet on total follicle number, the follicle distribution in the Old CR cohort more closely resembled that of young animals. The subset of Old CR animals that were still cycling, albeit irregularly, had more primordial follicles than controls ($P < 0.05$). Assessment of collagen and hyaluronic acid matrices revealed that CR attenuated age-related changes to the ovarian microenvironment. Overall, CR may improve aspects of reproductive longevity in the NHP, but the timing of when it occurs during the reproductive lifespan is likely critical.

INTRODUCTION

The ovary is one of the first organs to age in humans, with a significant decrease in fertility occurring when women reach their mid-30s due to decreased egg quality and continual follicle loss [1]. The age of onset of menopause is determined by the depletion of the ovarian follicle reserve [2], and this has important implications

for overall health since follicles produce estrogen which regulates numerous downstream organ systems [3]. In addition to loss of ovarian follicles, ovarian aging is also characterized by fibrosis of the ovarian stroma. Age-related fibrosis, or the thickening and stiffening of the extracellular matrix due to increased collagen and/or decreased hyaluronic acid, has been demonstrated in murine and human ovaries [4, 5]. The biological

sequelae of ovarian aging have significant societal and clinical ramifications as increasingly more women are postponing childbearing to older ages, [6] and more women are living longer post-menopause due to health and medical interventions [7]. Beyond physiologic aging, women with a prior history of medical conditions (e.g., prior ovarian surgery, chemotherapy, radiation therapy, severe endometriosis) or lifestyle factors associated with decreased ovarian function (e.g., smoking) are particularly at risk of a premature decline in their ovarian reserve and accelerated reproductive aging [1].

Given the tangible effects of ovarian aging, there is a need to establish interventions that improve reproductive longevity. Caloric restriction (CR) is a paradigm of extending longevity that was first described in the 1930s [8]. CR slows physiologic aging in many species, including fruit flies, fish, rodents, and nonhuman primates [9–15]. CR in mice is associated with other beneficial effects, including decreases in body weight, abdominal visceral fat, and insulin resistance [16]. Importantly, CR may also be a viable strategy to mitigate ovarian aging. The decreased metabolic rate and body weight that occur following CR have been shown to delay reproductive aging [17, 18]. In mice, CR maintains ovarian function into advanced ages, with higher numbers of ovarian follicles, decreased egg aneuploidy, and increased fecundity relative to controls [19]. Levels of 20% and 40% CR in female mice and rats, respectively, preserved the ovarian reserve [16].

Although the findings regarding CR in rodents are promising, they must be validated in a more relevant model prior to clinical translation. The female rhesus macaque (Macaca mulatta) is an ideal model for studying ovarian aging in primates. Rhesus macaques share ~93% of their genomic sequence with humans [20], and the reproductive anatomy and menstrual cycles of female macaques are similar to those of human females [21]. Importantly, rhesus macaques experience similar age-related ovarian changes as observed in women and female chimpanzees [23, 24]. Limited data have demonstrated that rhesus monkeys undergo menopause similar to women at approximately 25 years [25]. Unlike other laboratory animal models such as the rat and mouse, rhesus monkeys may be monitored for cessation of menstruation as is practiced clinically with human patients. Rhesus macaques have many similarities to humans, but the ability to define all environmental variables, including diet, is unique to NHP. Nonetheless, there are some differences between primates and humans

that may limit translatability. Macaques exhibit seasonal breeding patterns, in which reproductive hormonal levels and gonadal activity are synchronized with environmental cues, such as a photoperiod. The photoperiod or seasonal pattern can also lead to periodic fluctuations in the neuroendocrine system (hypothalamic-pituitary axis), confounding the observed age-related effect on reproductive or endocrine physiology [26–28]. Despite these considerations, NHP remain a valid and relevant model for humans.

CR intervention at a moderate level in rhesus monkeys has resulted in improvement in overall health and survival [20], including decreased fat, improved metabolism, and decreased risk for cardiovascular disease and diabetes [29]. The effect of CR on parameters of ovarian aging in primates, however, has not been systematically investigated. Thus, the goal of this study was to determine whether short-term (3 year) moderate CR administered in young and old rhesus macaques confers a beneficial effect on follicle dynamics and the extracellular matrix composition of the ovarian microenvironment.

RESULTS

### A nonhuman primate model of short-term moderate CR

To investigate the impact of CR and age on ovarian aging parameters, we acquired a subset of archived ovarian tissue samples from a prior study involving short-term moderate CR in the rhesus macaque in two age cohorts (Figure 1). In the "young" cohort, animals ranged in age from 7–10 years of age at the start of the study, and in the "old cohort" they ranged from 16–23 years of age at the start of the study (Figure 1). The animals were either maintained on a control diet (CON) or one of 30% CR (CR) for a period of three years after which necropsy was performed to harvest organs, including ovaries, for downstream analyses. At the time of necropsy, young animals were 12.3 ± 1.5 (control diet, $N = 4$) and 13.0 ± 0 years of age (CR diet, $N = 4$), and the old animals were 24 ± 2.5 (control diet, $N = 8$) and 23.7 ± 2.6 years of age (CR diet, $N = 5$) (Table 1). There was no significant difference in age at the time of necropsy based on diet group. The period of the study spanned adolescence and reproductive adulthood in the young cohort and reproductive adulthood, peri-menopause, and menopause in the old cohort (Figure 1). All young animals in both the CON and CR groups had regular cycles. Old animals were classified as either regular, irregular, or not cycling based on their hormone profile (Figure 1 and Table 1). There were no regularly cycling animals in the old CR group (Figure 1 and Table 1). No differences in estradiol (E2),

Table 1. Animal and ovarian tissue characteristics.

n	Young CON	Young CR		Old CON	Old CR	
	4	4		8	5	
Age at necropsy, years						
Mean ± S.D.	12.3 ± 1.5	13.0 ± 0.0	*ns*	24.0 ± 2.5	23.7 ± 2.6	*ns*
Range	(10–13)	(13–13)	*p* = 0.36	(19–26)	(20–26)	*p* = 0.86
			ns	1/8 Regular		*ns*
Menstrual cyclicity	4/4 Regular	4/4 Regular	*p* > 0.99	5/8 Irregular	4/5 Irregular	*p* = 0.67
				2/8 Non-cycling	1/5 Non-cycling	
Ovary weight, mg						
Mean ± S.D.	383.0 ± 130.1	379.8 ± 143.4	*ns*	243.6 ± 94.2	159.6 ± 62.9	*ns*
Range	(314–578)	(205–554)	*p* = 0.97	(145 - 377)	(72–226)	*p* = 0.11
Histologic slides generated, number						
Mean ± S.D.	442.5 ± 115.6	347.5 ± 88.5	*ns*	270.0 ± 77.1	278.0 ± 70.9	*ns*
Range	(320–560)	(220–420)	*p* = 0.24	(190–430)	(160–340)	*p* = 0.85

progesterone (P4), follicle-stimulating hormone (FSH) or luteinizing hormone (LH; relative to the LH peak) were noted among animals with regular cycles between young and old cohorts (data not shown). Thus, it appears that the CR diet permits normal functioning of the reproductive axis in young regular cyclers. By year 3 of the diet, the relative numbers of irregularly cycling and non-cycling animals increased in both the old CON
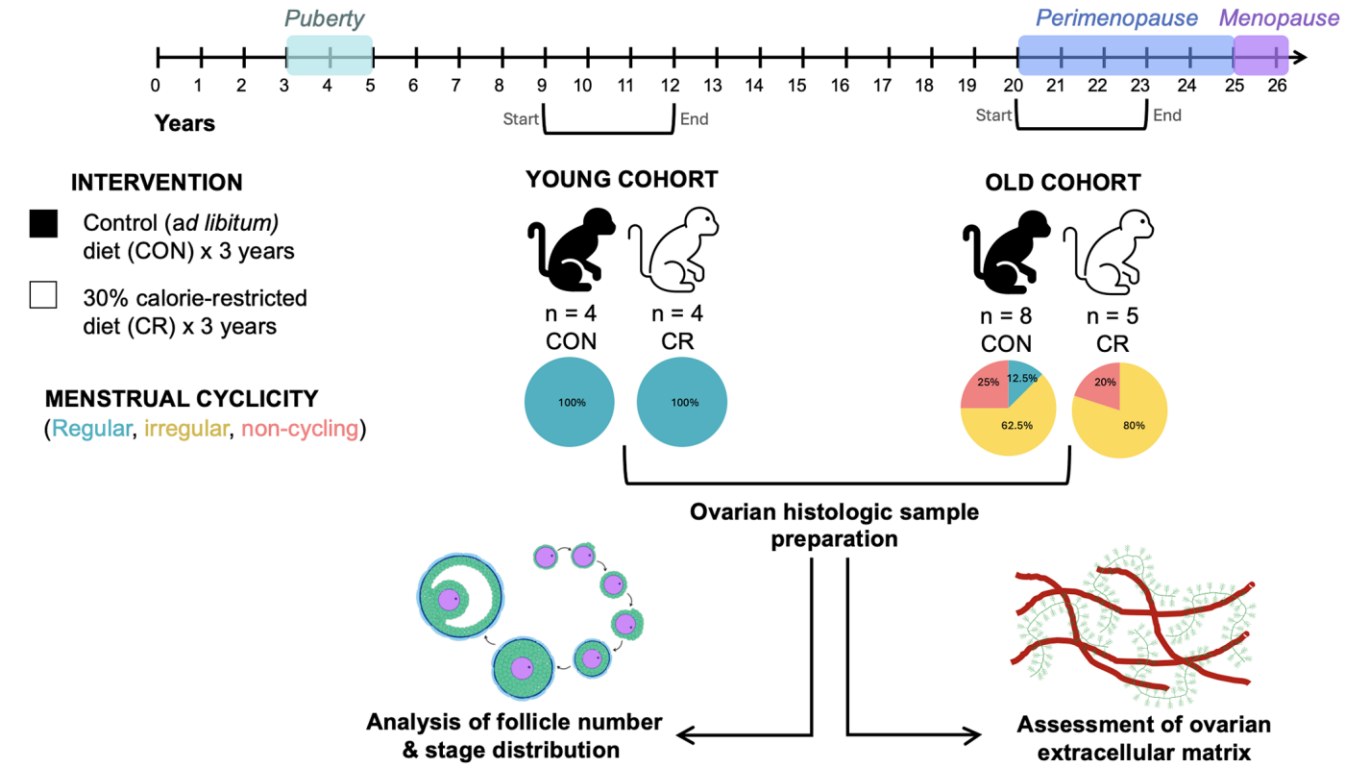
Figure 1. Schematic of caloric restriction paradigm. Animals were exposed to a moderate caloric restriction for up to 3 years. Animals in the young cohort were aged 7–10 years at the start of the study and age 10–13 years at necropsy. Animals in the old cohort were aged 16–23 years at the start of the study and age 19–26 years at necropsy. Animals' menstrual cyclicity was assessed using hormonal assays and observation of menses. Animals were classified as having regular cycles, irregular cycles, or non-cycling. All animals in the young cohort had regular cycles, while animals in the old cohort had regular cycles, irregular cycles, or were non-cycling. Following necropsy, ovarian tissue was harvested and prepared for downstream analyses of ovarian follicle number, follicular dynamics, and extracellular matrix composition. The timeline at the top of the image describes reproductive milestones in the rhesus macaque life cycle. Brackets beneath the timeline indicate the start and end of the study period for the two age cohorts.

and old CR groups due the animals entering perimenopause (Figure 1 and Table 1). Initiation of CR later in life did not appear to be beneficial to ovarian cyclicity as similar impairments occurred with age in both the old CON and old CR groups (Figure 1 and Table 1), however the small sample limits our ability to draw definitive conclusions.

The age-associated decrease in follicle number is not mitigated by CR, but CR exhibits a more youthful follicle class distribution in aged animals

To examine the effect of age and CR on ovarian aging parameters in the nonhuman primate, ovaries were harvested at the time of necropsy. The ovaries from young animals weighed more than those from old animals likely due to the greater number of follicles, but there was no difference within age cohort based on diet (Table 1). Consistent with the age-dependent difference in ovarian weight, we were able to obtain more histologic tissue sections (a surrogate marker for ovarian volume) following serial sectioning of young ovaries relative to old (Table 1). In mammals, the widely held dogma is that females are born with a finite and nonrenewable pool of primordial follicles which comprise the ovarian reserve and dictate reproductive lifespan [30]. These follicles are gradually depleted as females age, and at the time of menopause (cessation of ovarian cycling), very few follicles remain. When examining representative histological sections of the ovaries across experimental cohorts at a gross level,

there was an obvious age-dependent decline in the number of visible follicles as expected (Figure 2).

To gain further insight into how follicle dynamics in the rhesus macaque are impacted by age and diet, we classified and counted all the major follicle stages with normal morphology in the ovary (Figure 3). These included the quiescent pool of primordial follicles (Figure 3A) as well as those that had activated and were growing, including transitional primordial, primary, transitional primary, secondary, multilayer, and antral follicles (Figure 3B–3G). In addition to healthy follicles, we also classified and counted multi-oocytic follicles, secondary and multilayer follicles with abnormal morphological features, and atretic antral follicles (Figure 3H–3K). For each animal across experimental cohorts, we performed follicle counts in three histologic sections that spanned the ovary (Figure 3L, 3M). Follicle numbers were normalized to the area of the histological section, and each data point represented the average follicle number per area for each animal ($n = 3$ histological sections per animal) (Figure 4A–4H and Supplementary Figure 1A–1D). Overall, there was a decrease in total follicle number as a function of age for CON animals which is consistent with the gross histology (Figure 4A and Supplementary Table 1). For CON animals, there were significant decreases in primordial, transitional primordial, primary, transitional primary, secondary, and multilayer follicles between young and old animals (Figure 4B–4G). For CR animals, there were statistically significant
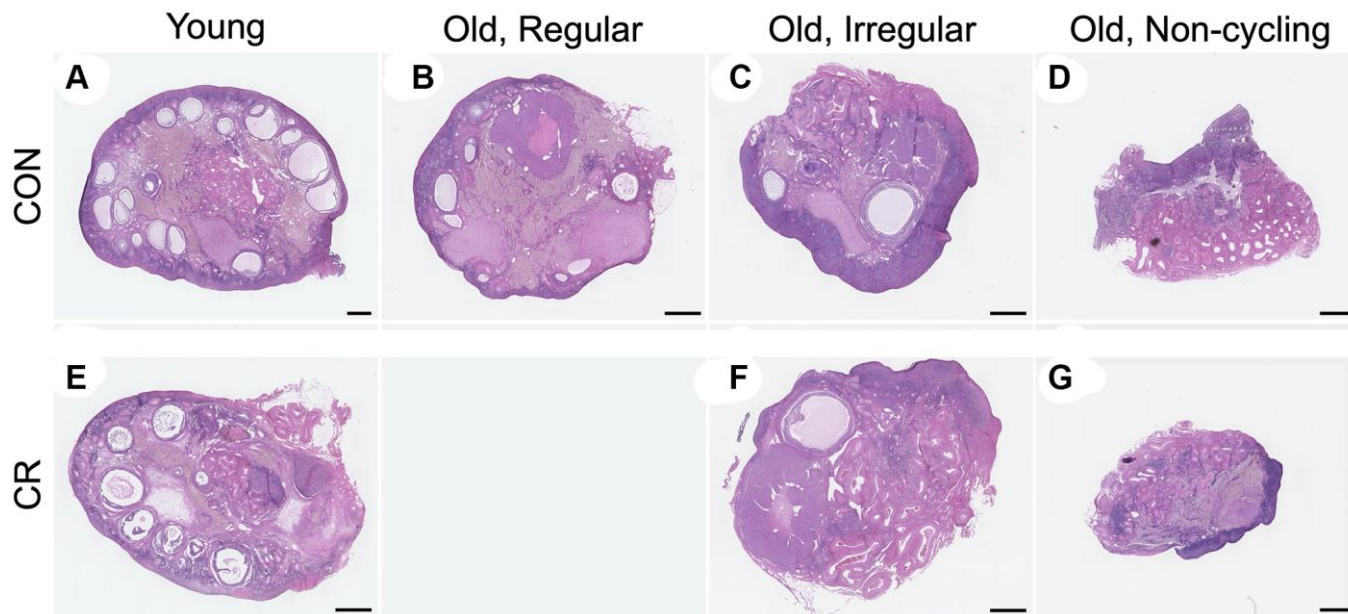
Figure 2. Representative histologic sections from young, old with regular cycles, old with irregular cycles, and old non-cycling animals exposed to control or calorie-restricted (CR) diet. Representative midsections from the following cohorts are shown: (**A**) young control, (**B**) old, regular cycling control, (**C**) old, irregular cycling control, (**D**) old non-cycling control, (**E**) young CR, (**F**) old, irregular cycling CR, (**G**) and old non-cycling CR. There were no old, regularly cycling CR animals. The scale bar is 1 mm.
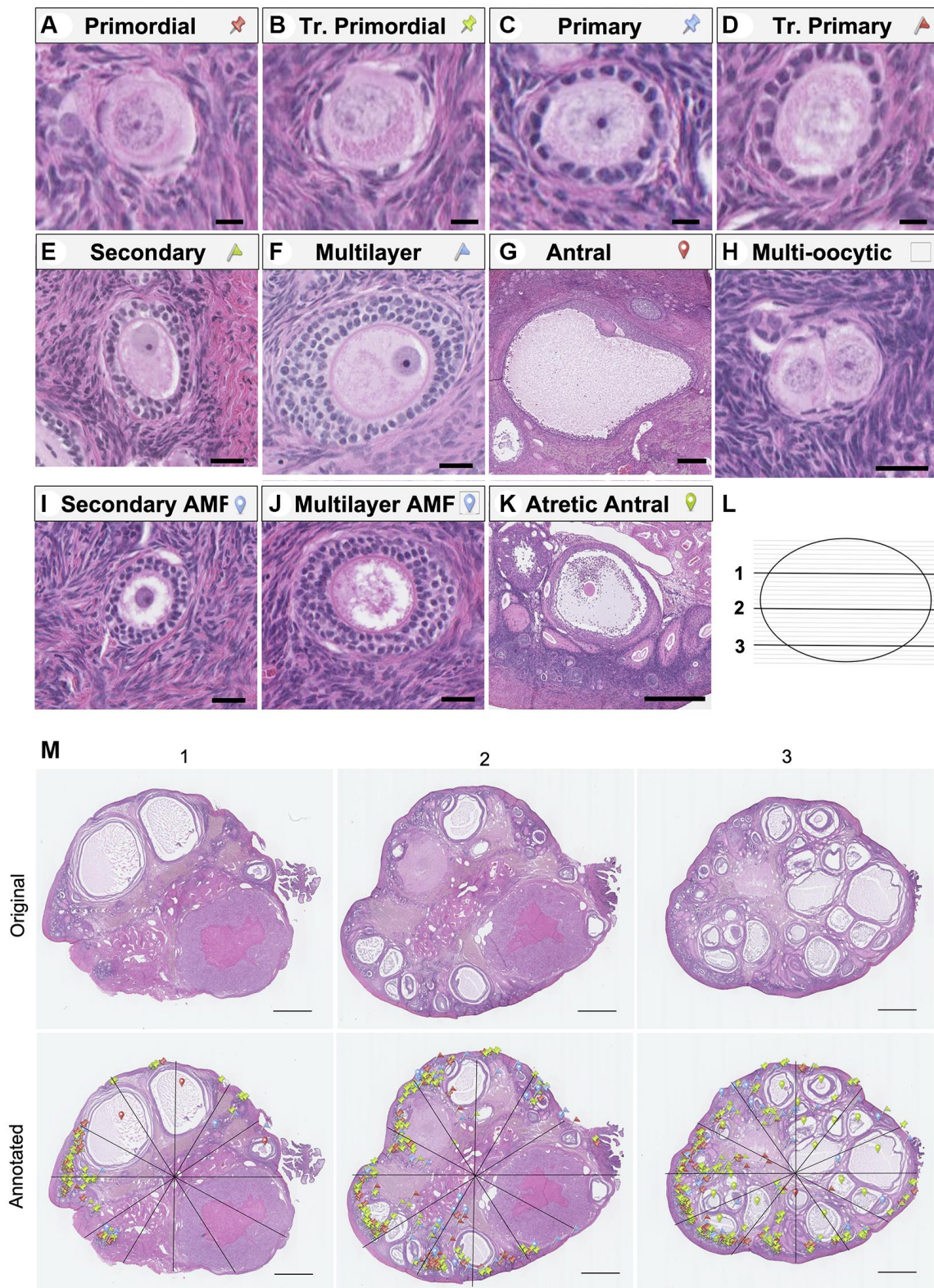
Figure 3. Representative images of follicle classes and follicle counting method schematic. Representative hematoxylin-and-eosin-stained images illustrating the following follicle classes are shown: (**A**) primordial, (**B**) transitional primordial), (**C**) primary, (**D**) transitional primary, (**E**) secondary, (**F**) multilayer, (**G**) antral, (**H**) multi-oocytic, (**I**) secondary with abnormal follicle morphology (AMF), (**J**) multilayer with AMF, (**K**) and atretic antral follicles. The follicle counting workflow depicting (**L**) the selection of representative ovarian sections from the top (1), middle (2), and bottom (3) quartiles of the ovary, and (**M**) schematic of follicle counting workflow, including dividing each section into twelve radial segments and annotation with colored markers as defined in A-K to mark and classify each follicle class. The scale bars are 10 μm (**A–D**), 25 μm (**E**, **F**, **H**, **I** and **J**), 250 μm (**G**), 500 μm (**K**), and 1 mm (**N**).
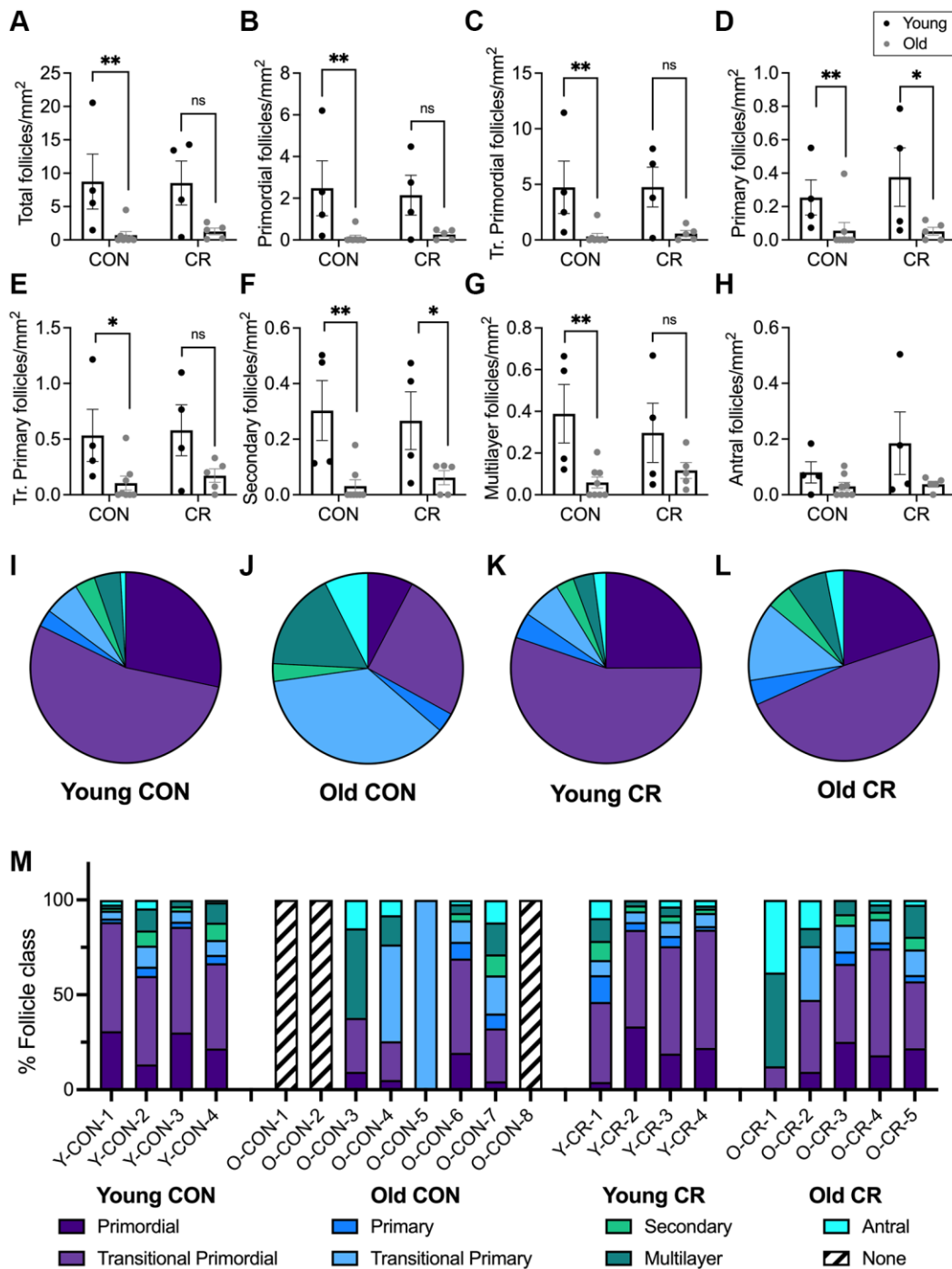
Figure 4. Follicle number per area differ between young and old animals and follicle class distribution and is affected by age and diet. Bar graphs of follicle number per ovarian section area for each normal follicle morphology class are shown for: (**A**) total number of follicles, (**B**) primordial, (**C**) transitional primordial, (**D**) primary, (**E**) transitional primary, (**F**) secondary, (**G**) multilayer, and (**H**) antral follicles. Pie charts show follicle class distribution for (**I**) young control, (**J**) old control, (**K**) young calorie-restricted, and (**L**) old calorie-restricted animals. Pie charts were generated by summing raw follicle number from each follicle class for all animals in an experimental group ((**I**) N = 4 animals, n = 3315 follicles, (**J**) N = 5 animals, n = 467 follicles, (**K**) N = 4 animals, n = 3448 follicles, and (**L**) N = 5 animals, n = 336 follicles) and plotted as pie charts to show follicle distribution across developmental classes. Data are shown as follicle number from each class summed for all animals in the given group (young control, young calorie-restricted, old control, old calorie-restricted). (**M**) follicle class distribution (shown as a percent) for individual animals. Animal identification codes are listed below the X-axis in panel M and can be cross-referenced to additional animal characteristics in Supplementary Table 2. Follicle number per area is plotted as untransformed data. Data are presented as mean ± SEM. Black circles indicate young animals, grey circles indicate old animals. Statistics were calculated on log-transformed data with a two-way ANOVA. Tukey's post hoc test was applied when one or both of the main effects were statistically significant. *$p ≤ 0.05$, **$p ≤ 0.01$. *P*-values for sources of variation of two-way ANOVA can be found in Supplementary Table 1.

decreases in primary follicles and secondary follicles between young and old animals (Figure 4D, 4F). Pairwise comparisons could not be made for antral follicles as there was no statistical significance for either of the main effects in the two-way ANOVA. Although there was a significant effect of age on follicle number across all follicle classes (except antral), there was no effect of diet on follicle number based on analysis of sources of variation using two-way ANOVA (Supplementary Table 1).

We performed an additional analysis of follicle number divided by total slide number per ovary, as a proxy for ovarian volume. As mentioned previously, we noted a large range of ovarian size across individual animals within an experimental group, as well as differences between groups, with ovarian mass significantly lower in old animals compared to young animals ($p = 0.0016$, Table 1 and Supplementary Table 2). Standardized follicle number was calculated by summing the follicle number per follicle class in each individual animal across all three tissue sections and dividing by the total number of histologic slides generated for that animal. Similar age-related declines in follicle number were observed when comparing these standardized follicle numbers (Supplementary Figure 2). No effect of diet on standardized follicle number was observed in the main effects analysis (Supplementary Table 3). Raw follicle number data is presented in Supplementary Table 4.

We next evaluated the distribution of follicles across the different developmental classes for each of the four experimental groups (Figure 4I–4L). The follicle class distribution for young CON, young CR, and old CR animals was grossly similar, with the vast majority being primordial or transitional primordial follicles (Figure 4I, 4K, 4L). By contrast, the follicle distribution in old CON animals was substantially different, with less than half of follicles classified as primordial or transitional primordial (Figure 4J). When compared to young animals, the follicle class distribution for old control animals is significantly different (X^2 (6, $N = 467$) = 234.6, $p <$ 0.0001). By comparison, there was no statistically significant difference in follicle class distribution between old calorie-restricted animals and young animals (X^2 (6, $N = 336$) = 12.54, $p = 0.0509$). We then plotted the follicle class distribution on the level of individual animals, which further demonstrates a similar follicle class distribution across the young CON, young CR, and old CR groups and confirms that these patterns are not due to particular animals (Figure 4M). Notably, this analysis revealed that the old CON animals appear quite distinct from the others given that 3/8 animals had no follicles and one had only transitional primary follicles in the analyzed histological sections (Figure 4M). Overall, these data suggest that although CR does

not prevent the overall age-dependent loss in follicles, it does maintain a distribution of follicles across developmental classes that is more similar to young animals, with a similar proportion of primordial and transitional primordial follicles observed between old CR animals and young animals irrespective of CON or CR status (Figure 4I–4M).

Menstrual cycle status is associated with follicle number

In our study, the cohort of old animals included one animal with regular cycles ($n = 1$ CON), nine with irregular cycles ($n = 5$ CON, $n = 4$ CR), and three non-cycling animals ($n = 2$ CON, $n = 1$ CR). We, therefore, performed an additional analysis of how follicle number per area is affected by diet and menstrual cyclicity (Figure 5 and Supplementary Figure 3). For all follicle classes, there was a clear pattern of decreasing follicle number per area with increased menstrual cycle irregularity, with the lowest numbers of follicles seen in non-cycling animals for both CON and CR animals (Figure 5A–5H and Supplementary Figure 1E–1H). This pattern was also seen for standardized follicle number (Supplementary Figure 3). Statistically significant decreases in follicle number per area of irregularly cycling or non-cycling control animals compared to regularly cycling control animals were seen for all follicle classes, except antral follicles (Figure 5). The two-way ANOVA revealed that there was no statistically significant interaction between the effects of diet and menstrual cyclicity for total follicle number per area as well as follicle number per area for all normal and abnormal follicle classes (Supplementary Table 5). Simple main effects analysis showed that diet did not have a significant effect on total follicle number per area as well as follicle number per area for all normal and abnormal follicle classes (Supplementary Table 5). However, simple main effects analysis did show that menstrual cyclicity had a significant effect on the total follicle number per area, primordial follicle number per area, transitional primordial follicle number per area, primary follicle number per area, transitional primary follicle number per area, secondary follicle number per area, multilayer follicle number per area, multi-oocytic follicle number per area and atretic antral follicle number per area (Supplementary Table 5). Similar results in the main effects analysis were seen when looking at standardized follicle counts (Supplementary Table 6).

Caloric restriction maintains the primordial follicle pool in a subpopulation of animals with irregular cycles

Previous studies have shown that the timing of CR interventions can modulate their impact [31, 32].

Although many studies focus on early (pre- or peri-pubertal) intervention [33–35], those aimed at extending the fertile window are likely to be to be more clinically relevant if initiated in later adulthood, when fertility is beginning to decline. Given the physiologic differences between aged animals with and without menstrual cycles, we performed a more focused analysis on the subgroup of irregularly cycling animals to determine the effect of CR in this clinically relevant population (Figure 6 and Supplementary Figure 1I–1L). Despite the lack of statistically significant effect of diet on follicle number in the cohort of all aged animals, it was physiologically reasonable to perform this subgroup analysis, given the significant physiological differences between cycling and non-cycling animals, and the statistically significant effect of menstrual cyclicity on follicle number. In the subgroup of irregularly cycling old animals, CR animals had significantly higher total follicle numbers per area than control (Figure 6A) which was primarily attributed to the significant increase in the number of primordial and multilayer follicles per area (Figure 6B, 6G), while other follicle classes did not differ (Figure 6C–6F, 6H). Despite the small follicle numbers in the abnormal follicle groups, which limits the power of the study, a significant increase in the secondary AMF follicle number per area in CR females was observed (Supplementary Figure 1J). However, a similar trend toward increasing follicle number per area with CR was seen for multilayer AMF follicles and atretic antral follicles (Supplementary Figure 1K, 1L). There was no effect of diet on multi-oocytic follicle number per area (Supplementary Figure 1I). Standardized follicle number for total follicles, follicles with normal morphologies, and follicles with abnormal morphologies are presented in Supplementary Figure 4. There was a statistically significant increase in only primordial follicle number with CR using this analysis (Supplementary Figure 4B), while total follicle number and other follicle classes did not differ (Supplementary Figure 4A, 4C–4L). Thus, a CR intervention later in life when an individual is experiencing irregular menstrual cyclicity may have a positive impact by preserving the primordial follicle pool and thereby potentially prolonging reproductive function.

Age-related ovarian fibrosis is attenuated by CR

Distinct changes in the ovarian extracellular matrix occur with advanced reproductive age, including an increase in collagen and a decrease in hyaluronic acid which are associated with increased tissue stiffness [4, 36, 37]. To investigate whether CR had an impact on age-related changes in ovarian extracellular matrix, we evaluated collagen and hyaluronic acid (HA).
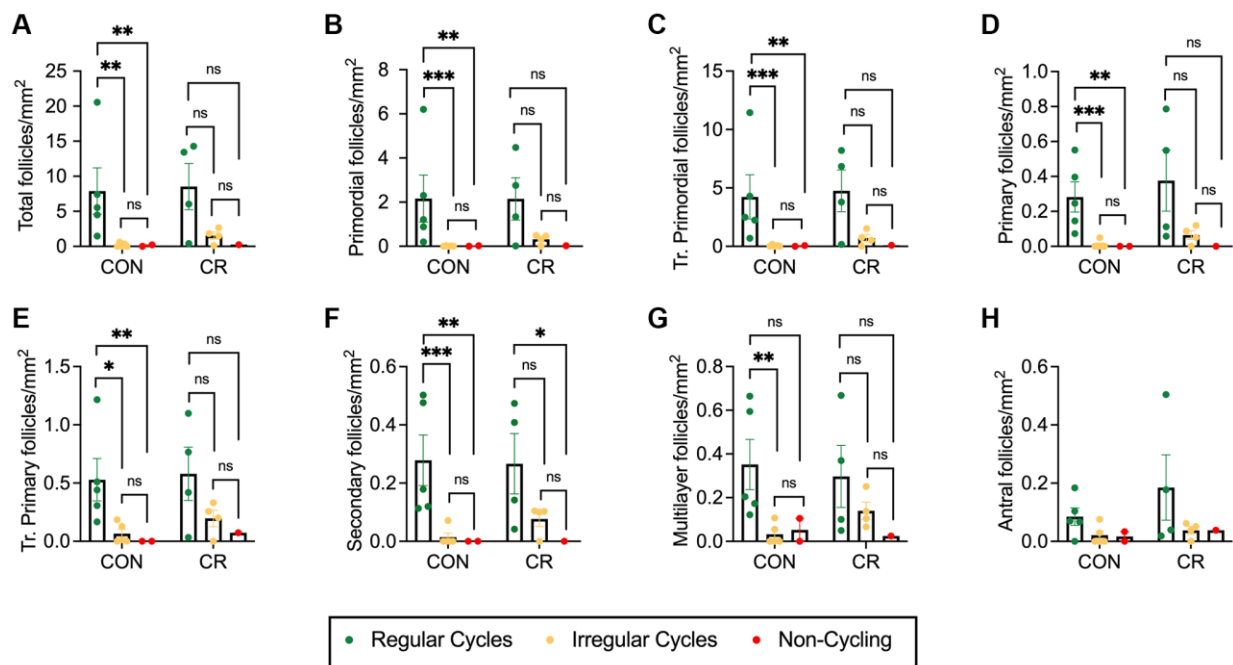
Figure 5. Follicle number per area as a function of reproductive status. Bar graphs showing follicle number per area for each normal follicle morphology class: (**A**) total number of follicles, (**B**) primordial, (**C**) transitional primordial, (**D**) primary, (**E**) transitional primary, (**F**) secondary, (**G**) multilayer, and (**H**) antral. Follicle number per area is plotted as untransformed data. Data presented as mean ± SEM. Green circles represent animals with regular cycles, yellow circles represent animals with irregular cycles, and red circles represent non-cycling animals. Statistics were calculated on log-transformed data with a two-way ANOVA. Tukey's post hoc test was applied when one or both of the main effects were statistically significant. *$p \leq 0.05$, **$p \leq 0.01$, ***$p \leq 0.001$. P-values for sources of variation of two-way ANOVA can be found in Supplementary Table 5.

We performed Picrosirius Red staining which is a histologic stain that can be used to detect collagen I and III fibers, and we used quantitative digital pathology to quantify pixels of high, medium, and low intensity in ovarian sections across experimental groups, based on our prior work (Figure 7) [38]. As expected with age, there was an increase in collagen content in old CON ovaries (Figure 7B, 7F) relative to young CON ovaries (Figure 7A, 7E) as evidenced qualitatively by the increase in red staining and quantitatively by the age-dependent increase high intensity pixels (Figure 7D, 7H, 7K) with no CR effects in young animals (Figure 7C, 7G). However, this age-dependent increase in ovarian collagen was abrogated in ovaries from old CR animals (Figure 7K). With increased age, there was a decrease in medium intensity pixels in control animals, suggesting a change in the collagen matrix (Figure 7J). No statistically significant differences between groups were seen for low intensity pixels (Figure 7I). In the aging mouse and human ovary, the increase in collagen is accompanied by a decrease in hyaluronic acid [4, 36, 39]. Using a fluorescent hyaluronic acid binding protein (HABP) assay to localize hyaluronic acid within ovarian sections, we noted that the loss of hyaluronic acid with age is also conserved in the rhesus macaque in CON samples (Figure 8A, 8B). However, this age-related difference was not significant in CR animals (Figure 8C–8E). Together these results suggest that CR may attenuate age-related fibrosis in the ovary.

DISCUSSION

In this study, we provide evidence that short-term moderate CR confers a beneficial effect on reproductive longevity in the NHP model but may be dependent on the timing of when CR is administered with respect to the reproductive lifespan of the animal. CR preserved a more youthful distribution of follicles among aged animals through preservation of a higher proportion of primordial follicles, while not necessarily attenuating the overall declining number of follicles. We established that CR maintains the number of primordial follicles in irregularly cycling animals, supporting the notion of CR timing as a modulator of ovarian impact. Finally, we found that CR attenuates age-related changes in collagen and hyaluronic acid matrices which are both implicated in ovarian fibrosis. These main findings suggest that CR may improve reproductive longevity, with timing as a critical factor. Moreover, our study established a novel follicle-class categorization method for the NHP model which is critical for future studies that rely on this important ovarian endpoint. This study also defines the age-related decline in follicle number both in cycling and non-cycling animals and provides a quantitative metric of reproductive longevity in the NHP model.

There is a large degree of variation in the existing literature with respect to the age of onset, duration, and
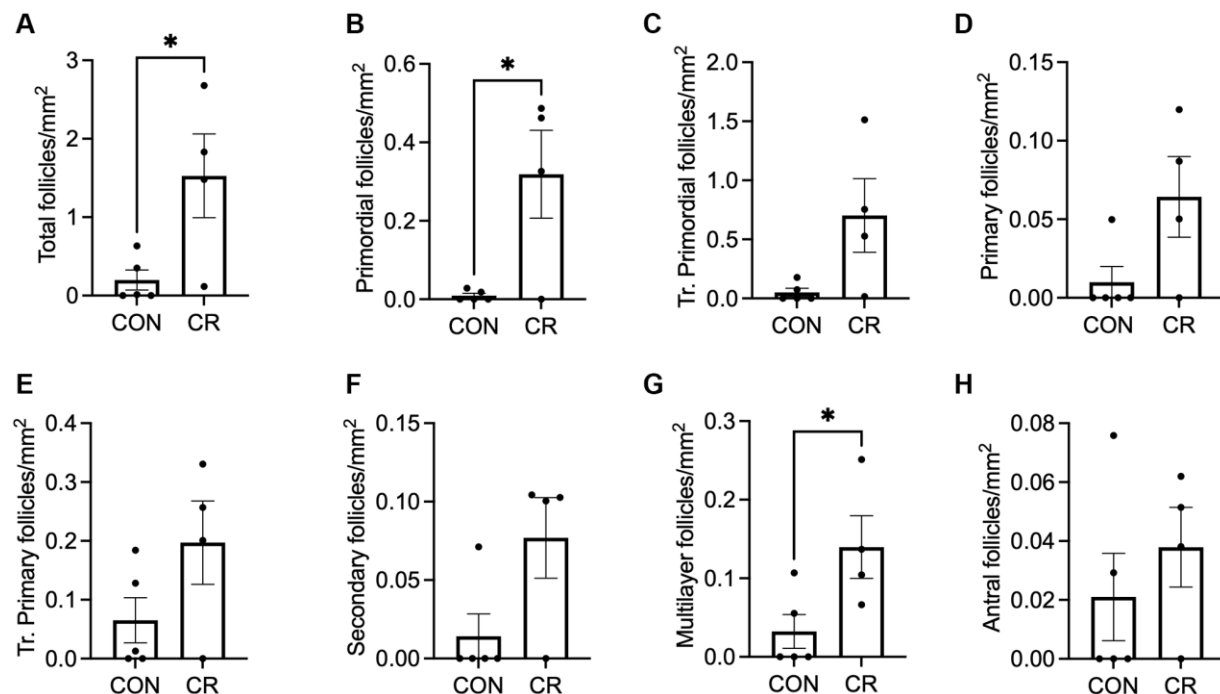
Figure 6. Follicle number per area as a function of diet in old animals with irregular cycles. Bar graphs of follicle number of normal morphology per ovarian section area are shown for the following classes: (**A**) total number of follicles, (**B**) primordial, (**C**) transitional primordial, (**D**) primary, (**E**) transitional primary, (**F**) secondary, (**G**) multilayer, and (**H**) antral follicles. Data are presented as mean ± SEM. Statistics were calculated using an unpaired *t*-test. *$p ≤ 0.05$.

degree of the CR intervention. The data demonstrate that the timing of the CR intervention matters and may be species-specific. Early onset CR in rodents increased longevity compared to adult-onset CR [33, 35]. Yet, CR implemented in NHP juveniles does not seem to improve survival or longevity [14]. Hence, while CR
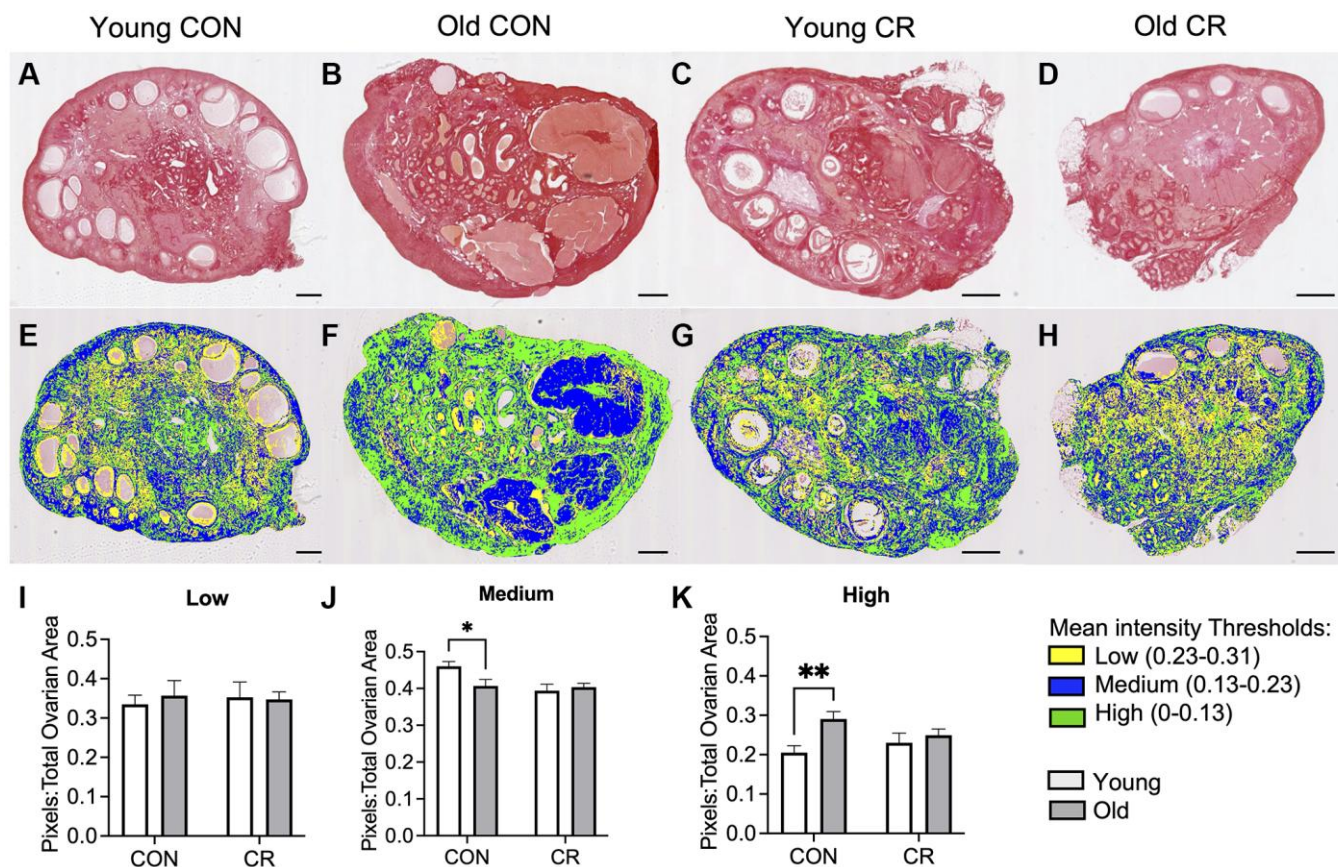
Figure 7. Assessment of collagen I and III in histologic ovarian sections using Picrosirius red (PSR). Representative images of PSR stained ovarian tissue sections for (**A**) young control, (**B**) old control, (**C**) young calorie-restricted (CR), and (**D**) old calorie-restricted (CR). Corresponding representative images of the quantitative histology algorithm showing intensity of PSR staining, where low intensity pixels are shown in yellow, medium intensity pixels are shown in blue, and high intensity are shown in green for (**E**) young control, (**F**) old control, (**G**) young calorie-restricted (CR), and (**H**) old calorie-restricted (CR). Bar graphs showing quantification of (**I**) low intensity, (**J**) medium intensity, and (**K**) high intensity pixels. An $N = 3$ images per animal and $N = 4–8$ animals per experimental group were analyzed. Data are presented as mean ± SEM. Statistics were calculated using a two-way ANOVA with Sidak's multiple comparison test. $^*p \leq 0.05$. $^{**}p$ 0.01. The scale bar is 1 mm.
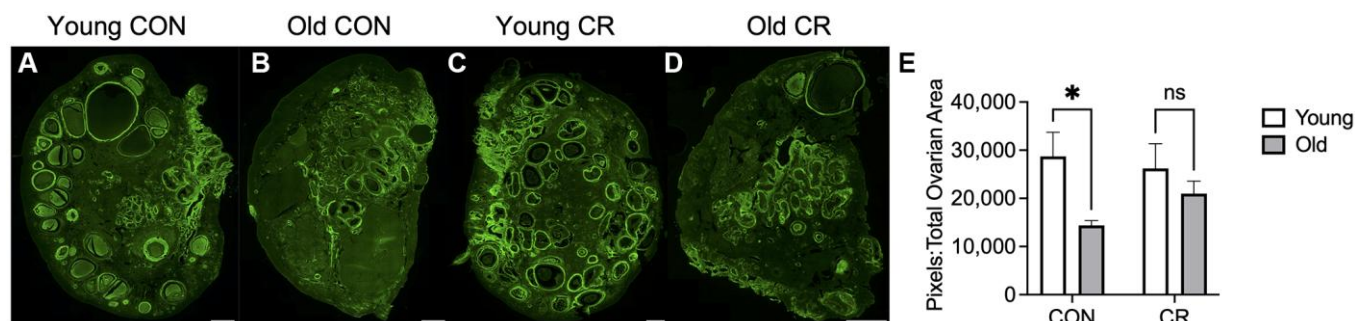
Figure 8. Hyaluronic acid binding protein localization in ovarian tissue sections. Representative fluorescent microscopy images of hyaluronic acid binding protein (HABP) showing localization of hyaluronic acid in ovarian tissue sections in (**A**) young control, (**B**) old control, (**C**) young calorie-restricted (CR), and (**D**) old calorie-restricted (CR) animals. Quantification of the positive pixels per area is shown in (**E**) with $N = 3$ images per animal and $N = 4–8$ animals per experimental group. Data are presented as mean ± SEM. Statistics were calculated using a two-way ANOVA with Sidak's multiple comparison test. $^*p \leq 0.05$. The scale bar is 1 mm.

effectively delays the effects of aging in NHP, the extent of CR benefits relates to the age of onset of the CR intervention [20]. Our study supports previous studies in NHP, that CR in young cohorts may not necessarily improve reproductive longevity and supports the notion that the age of onset of CR matters. Moreover, we propose a novel notion that menstrual status during ovarian aging, rather than age alone, may play an important role in the impact of CR on the declining ovarian reserve.

In our study, we investigated a short-term (3 year) period of CR. Studies in rodents have reported long-term CR interventions, with some studies even reporting life-long moderate CR [40]. Prior studies in rhesus macaques carried out by the National Institute on Aging (NIA) and Wisconsin National Primate Research Center (WNPRC) have reported decades-long CR inter-ventions, with mixed effects [14, 20]. Such long-term CR is likely not sustainable or realistic in NHP or humans, and some have raised concerns about the safety of such long-term interventions, with regards to bone mineral density, impaired immune function, and nutrient deficiencies [41]. Intermittent fasting may offer an more acceptable, feasible alternative to long-term caloric restriction and studies have shown beneficial effect on ovarian aging parameters in mice [42]. The impact of intermittent fasting in primates remains to be determined. Finally, the degree of CR is an important consideration. CR at a higher level of 40% delayed ovulation in macaques through an endocrine effect caused by a negative energy balance [43]. Our study's use of 30% CR suggests a similar level of diet restriction impacts ovarian mechanisms in NHP. Further research is needed to determine the minimum degree of CR that confers a benefit in NHP.

The exact mechanisms by which CR exerts its anti-aging effects and promotes ovarian longevity remain unknown. However, the beneficial effects of CR are likely multi-factorial, including positive effects on insulin sensitivity, inflammation, energy metabolism, oxidative stress, autophagy, and the neuroendocrine axis [44, 45]. Multiple molecular pathways have been hypothesized to be involved, including mTOR and the related SIRT pathways [46]. Indeed, other studies have analyzed pharmacologic interventions such as rapamycin, which maintain the ovarian reserve through mTOR inhibition [47] and sirtuin-activating compounds [48], which reduced oxidative stress through the sirtuin pathway. Our results show that CR attenuates the ovarian age-related fibrotic process. Metformin, a common anti-diabetic medication, has also been shown to decrease ovarian fibrosis [49, 50]. Studies have shown that the reduction of ovarian fibrosis through anti-fibrotic drugs has been shown to extend female reproductive lifespan

via an increase in ovulation capacity in a mouse model [51]. Therefore, because CR attenuates fibrosis in the NHP model, it may further suggest CR as a tool to extend reproductive lifespan, as the fibrotic process is directly linked to ovulation capacity. Further studies identifying the mechanisms of CR underlying the regulation of ovarian lifespan are needed so that therapeutic approaches to target these pathways may be developed to maintain ovarian reserve.

Limitations of this study include the retrospective nature of analysis and non-uniform group sample sizes. Rhesus macaques, like humans, are genetically hetero-geneous and may therefore display varied phenotypes in response to the same environmental stimuli [20]. For example, animals progressed through their reproductive lifespans spontaneously, so number of animals regularly-cycling, irregularly cycling, and non-cycling was not consistent between experimental groups. Finally, our study analyzed the impact of only one level of CR (30% caloric restriction) and does not address the impact of different degrees of CR, which may be an important modulator of its effect on ovarian longevity. Another limitation is that only a subset of histological sections was analyzed per animal. Use of sampling strategies (counting a subset of histological sections and applying a correction factor to account for uncounted tissue), is a common approach in the follicle counting literature and as long as same technique is applied uniformly to all experimental groups, results in internal validity [52].

In our study, although CR did not significantly increase the overall number of follicles, CR maintained a youthful proportion of follicle class, preserved primordial follicles in irregularly cycling animals, and attenuated ovarian fibrosis. The clinical implications are relevant, and our study provides evidence of CR as a possible intervention to attenuate the loss of ovarian function with aging. Through the NHP model, we provide findings that can be extended to humans more specifically than other model systems. The impact of the relationship between CR and other molecular pathways on ovarian aging remains to be determined, but may provide an important insight to the mechanism of CR as an intervention and support the use of CR mimetics. Optimal timing, duration, and degree of CR intervention needed to promote reproductive longevity in women remains to be determined by future studies.

MATERIALS AND METHODS

Animals

We acquired a subset of archived ovarian tissue samples from a prior study involving short-term moderate CR in

the rhesus macaque in two age cohorts (Figure 1). In this study, a cohort of young and old (peri-menopausal) female rhesus macaques (*M. mulatta*) was selected under a protocol approved by the Institutional Animal Care and Use Committee (IACUC) of the Oregon National Primate Research Center. The animals were housed in individual cages with auditory, visual, and olfactory interaction with female conspecifics in a temperature-controlled environment (24°C) under a fixed 12L:12D photoperiod (lights on from 700 h to 1900 h) with *ad libitum* access to drinking water. Animals were cared for by the Oregon National Primate Research Center in accord with the National Research Council's Guide for the Care and Use of Laboratory Animals [53], which included daily health checks to ensure normal behavior, food consumption, and waste production. Additionally, routine physical examinations, hematological studies, fecal parasite checks, tuberculin testing, and dental cleaning were performed periodically.

Diet information

Animals in both the young and old cohorts were randomly assigned to control (CON) or caloric restriction (CR) diet. While the original CR studies in rodents performed by McCay et al. [8] use a 40% caloric restriction, when designing this study for non-human primates, a 30% reduction in calories was decided upon based on considerations of safety, compliance, and ability to perform the intervention in juvenile animals still in their growth phase when translation of McCay's seminal work to a larger animal species. The experimental cohorts for this study included: (1) young/CON (young animals on the control diet; $N = 4$), (2) young/CR (young animals on the caloric restriction diet; $N = 4$), (3) old/CON (old animals on the control diet; $N = 8$), (4) old/CR (old animals on the caloric restriction diet; $N = 5$) (Figure 1 and Table 1). Animals in the control group were provided a daily allotment of food, adjusted for age and body weight. The average daily value was then divided into two meals. The CR diet was then reduced by 10% per month until a 30% CR was achieved as previously described [31, 32, 54, 55]. CR animals received 30% less food than age- and body weight-matched CON animals. Each animal received a measured portion of specially formulated biscuits (Cargill, Minneapolis, MN, USA) supplemented with daily fresh fruits or vegetables (10–40 cal) and was fed twice daily, at 0800 h and 1500 h. Biscuit composition was 15% protein, 5% fat, and 5% fiber, with a caloric content of ~3.7 kcal/g. To avoid any deficiencies in essential nutrients in the CR animals, the diet was enriched with a vitamin/mineral mix that was 40% higher than the recommended allowance for rhesus macaques by the

National Research Council [53]. These animals were calorie restricted but not malnourished. Animals were maintained on a control (CON) or a moderate CR diet for up to 3 years. Biochemical assays were performed periodically and with every new shipment to ensure diet content and quality [56, 57].

Menstrual cyclicity analysis

We used hormone data from the Endocrine Services Laboratory Core, Oregon National Primate Research Center (Roche, Beaverton, OR, USA) to assign animals into groups of those who had regular cycles and those that did not. Steroid (estradiol (E2), progesterone (P4)) and gonadotropin hormones (follicle-stimulating hormone (FSH), luteinizing hormone (LH)) were retrospectively synchronized relative to the estimated mid-cycle LH peak (designated LH d0). This separates the follicular and luteal phases to permit analyses between comparable physiological states. Based on these data, animals were assigned to one of two groups: regular cyclers and irregular cyclers. Regular cyclers exhibited 3 cycles each demonstrating a mid-cycle E2 peak followed by luteal phase levels of P4 during the 90-day interval. Irregular cyclers typically exhibited at least one cycle within the 90-day interval with a mid-cycle E2 peak followed by basal levels of P4 indicating the absence of a luteal phase. The remaining two cycles within the 90-day interval were characterized by very low levels of E2 and P4 lacking cyclic rises, with no further observation of menses. Non-cycling animals displayed very low hormone activity, with no recorded menses noted and little to no change in both E2 and P4. After the 90-day sampling period (between 1–2 years on CR), menses records were reported every month until the completion of the experiment at the end of three years. Using the definition from Gilardi and colleagues [25], an animal was classified as an irregular cycler if she exhibited 6 consecutive months or more of irregular cycles, excluding the non-breeding season (June through August). Data on hormone levels and response to ovarian stimulation will be presented in an accompanying manuscript.

Histological samples

At the end of the study period, animals were sacrificed, and ovaries were harvested. Ovaries were fixed in 4% paraformaldehyde (Sigma-Aldrich, St. Louis, MO, USA) for 24 hours at 4°C, 4% sucrose (Sigma-Aldrich, St. Louis, MO, USA) for 24 h at 4°C, and stored in 70% ethanol (DeCon Labs, Inc., King of Prussia, PA, USA) at 4°C for up to one week prior to dehydration and embedding in paraffin. The ovaries were serially sectioned at 5 μm thickness and mounted onto slides with two sections per slide. As it has been previously

demonstrated that the number of primordial follicles did not differ between right and left ovaries in rhesus macaques only one ovary per animal was serially sectioned and used for histological analysis in this study [58]. These slides were used for downstream analyses as described below.

Follicle classification and counting

A subset of histological sections (every 10th slide) was stained with hematoxylin and eosin (H&E) to visualize ovarian follicles and other tissue structures. Samples were deparaffinized in Citrosolv (Decon Laboratories, King of Prussia, PA, USA) and rehydrated in a series of graded ethanol baths (100%, 75%, 70%) and a standard H&E staining protocol was used. H&E-stained slides were imaged using the NanoZoomer Digital Pathology System HT-9600 (Hamamatsu, Hamamatsu City, Japan). Images were then accessed using NDP Viewer Software (Hamamatsu, Hamamatsu City, Japan). Follicle counting was performed in the NDP Viewer software under 40X magnification. To account for variation in ovary size and tissue architecture, three representative sections per animal were selected for analysis at one quarter (1), midway (2), and three quarters (3) through the ovary (Figure 3L). Each section was radially divided into 12 wedge-shaped segments to facilitate counting (Figure 3M). Within each segment, each follicle type was assigned a colored marker based on the classification system described below. Three individual counters counted a section at the same location in the ovary across all animals (e.g., section 1, 2, or 3, Figure 3L). To ensure rigor and reproducibility, for every 12 samples analyzed (top, middle, and bottom section from an animal in each of the four experimental groups), a calibration count was performed as follows. For each section 1, 2, or 3, an individual counter blinded to the original count re-analyzed one wedge-shaped segment from the section. Thus, three wedges per 12 histological samples were re-analyzed. *A priori* it was established that total follicle counts must be within 5% error, or the entire histological section was reanalyzed by the second counter, and counts were then averaged. No histological sections met the requirement for reanalysis by a second counter. Follicle counts were totaled and reported by follicle class.

The protocol for classifying follicles for counting purposes was adapted for NHP based on categories established during discussions held at the 2021 Ovarian Anatomy Nomenclature Workshop led by the National Institutes of Health [59]. For morphologically normal follicles, a primordial follicle was defined as having an oocyte surrounded by a complete or incomplete layer of squamous granulosa cells (Figure 3A). A transitional primordial follicle was one that has an oocyte sur-

rounded by a complete or incomplete layer of both squamous and cuboidal granulosa cells (Figure 3B). A primary follicle contained an oocyte surrounded by only cuboidal granulosa cells which formed a compact and complete (or nearly complete) layer (Figure 3C). A zona pellucida between the oocyte and granulosa cells was also visible at this stage. A transitional primary follicle consisted of an oocyte surrounded by more than 1, but fewer than 2 complete layer(s) of cuboidal granulosa cells (Figure 3D). Follicles were classified as secondary when the oocyte was surrounded by 2–3 layers of cuboidal granulosa cells and multilayer when surrounded by 3+ such layers (Figure 3E, 3F). Classification was based on the maximum number of layers on any given side of the follicle. Antral follicles were large and contained a fluid-filled antral cavity which spanned multiple sections (Figure 3G). An outer layer of theca cells was typically visible in follicles at the secondary stage and beyond and was distinctly formed in antral follicles. To avoid double counting follicles, antral follicles were not counted in the middle section of each animal. Otherwise, follicles were classified regardless of the presence of an oocyte nucleus, as the sections analyzed were sufficiently far apart.

In addition to morphologically normal follicles, we also classified and quantified follicles with abnormal morphological features. A multi-oocytic follicle contained two or more oocytes within one follicle structure enclosed by a basement membrane (Figure 3H). A secondary or multilayer follicle with abnormal morphological features (secondary AMF, multilayer AMF) contained structural abnormalities in the oocyte and/or granulosa cells, such as the presence of vacuoles in more than 50% of the oocyte (Figure 3I, 3J). Other criteria leading to an AMF classification included a damaged, misshapen, or degenerating oocyte, nucleus, and/or granulosa cells, or the severe shrinkage of the oocyte and/or granulosa cells away from the stroma in a section where most follicles were clearly identifiable suggesting that the phenotype was not a fixation artifact. Atretic antral follicles were defined as those with significant numbers of granulosa cells which had separated from the mural layer and localized within the antral cavity. Atretic antral follicles typically also exhibited other AMF features in the nucleus, oocyte, and/or granulosa cells (Figure 3K). Follicle number per area was calculated by dividing the follicle number by the area of the histologic section, which was measured using Fiji (ImageJ, National Institutes of Health, Bethesda, MD). Standardized follicle number was calculated by summing the follicle number per follicle class in each individual animal across all three tissue sections and normalizing to the total number of histologic slides generated for that animal. To generate the pie charts in Figure 4I–4L, raw follicle number from

each follicle class was summed for all animals in a given experimental group and these sums were plotted to show the distribution of follicles from each class. As there are different numbers of animals in each experimental group and different numbers of follicles counted for each animal, each pie chart depicts the follicle distribution for a different number of animals/follicles (for: (I) $N = 4$ animals, $n = 3315$ follicles); (J) $N = 5$ animals, $n = 467$ follicles); (K) $N = 4$ animals, $n = 3448$ follicles; and (L) $N = 5$ animals, $n = 336$ follicles). Animals without follicles were not included in pie charts.

Picrosirius red staining and collagen quantification

For assessment of collagen I and collagen III, ovarian sections ($N = 4$–8 animals/group, $N = 6$ sections/ovary) were stained with Picrosirius Red (PSR) according to established protocols [36]. Briefly, tissue sections were deparaffinized in Citrosolv (Decon Laboratories) and then rehydrated in a series of graded ethanol baths (100%, 70%, and 30%). Slides were submerged in a PSR staining solution, which was prepared by dissolving Sirius Red F3B (Direct Red 80, Color Index 35780, Sigma-Aldrich, St. Louis, MO, USA) in a 1.3% saturated aqueous picric acid solution (Sigma-Aldrich, St. Louis, MO, USA) at 0.1% w/v. Slides were immersed in the PSR staining solution for 30 minutes at room temperature, then destained with acidified water. Samples were then rapidly dehydrated in 100% ethanol, cleared in xylene, and mounted with synthetic mounting media. Quantitative digital microscopy was used to analyze the collagen content in the PSR-stained tissue sections as previously described [38]. Stained slides were imaged using the NanoZoomer Digital Pathology System HT-9600 (Hamamatsu, Hamamatsu City, Japan). Images were then imported into Visiopharm software (Visiopharm, Hoersholm, Denmark) and analyzed using the Image Analysis Module. Three slides (top, middle, and bottom) with two adjacent sections were analyzed for each animal. Regions of interest (ROIs) were drawn around each ovarian tissue section and assigned to "right" or "left" ovary. Then, these images were converted into grayscale values using the Chromaticity Green feature band. The software labeled each pixel as low, medium, or high degree of staining based on thresholds used in our prior work [38]. Images were processed in batch mode using this algorithm. The area of pixels with low, medium, and high staining intensity was calculated per total ovarian area and averaged between left and right ovarian sections.

Hyaluronic acid binding protein assay and hyaluronic acid quantification

A hyaluronic acid binding protein (HABP) assay was performed to localize hyaluronic acid within histological sections of ovarian tissue as previously described [39, 60]. In brief, tissue sections were deparaffinized in Citrosolv (Decon Laboratories) and then rehydrated in a series of graded ethanol baths (100%, 95%, and 95%). Slides were incubating in running reverse-osmosis water for 1 minute and washed in 1X phosphate buffered saline (PBS) with gentle rocking for 10 minutes. An Avidin/Biotin Blocking Kit (Vector Laboratories, Burlingame, CA, USA) was used according to kit instructions to block endogenous avidin and biotin within the tissue sections. Avidin was applied for 15 minutes at room temperature. Unbound avidin was rinsed off using 1X PBS, then biotin was applied for 15 minutes at room temperature. Unbound biotin was rinsed off using 1X PBS and slides were subsequently incubated in normal goat serum (Fisher Scientific, Waltham, MA, USA) for 20 minutes. Next, 1 mg/mL hyaluronidase (Sigma-Aldrich, St. Louis, MO, USA) in saline solution was applied to negative control tissue sections and saline alone was applied to experimental sections. Tissue sections were incubated in a humid chamber for 1 hour at 37°C. After rinsing in 1X PBS, biotinylated HABP (Calbiochem, San Diego, CA, USA) diluted in normal goat serum was applied to all sections and incubated for 1 hour at room temperature. Slides were again washed in 1X PBS. To amplify signal, slides were incubated in ABC reagent (Vector Laboratories, Burlingame, CA, USA) for 30 minutes at room temperature, followed by TSA Plus Fluorescein System (Akoya Biosciences, Marlborough, MA, USA) at a 1:400 dilution for 5 minutes at room temperature. All incubations were performed within a humified chamber. Samples were mounted in Vectashield HardSet Antifade Mounting Medium with DAPI (4′,6-diamidino-2-phenylindole; Vector Laboratories, Burlingame, CA, USA) to counterstain cell nuclei. Sections were processed in batches containing one slide from each animal. The HABP assay was performed on three replicates from each animal. Entire ovarian tissue sections were scanned at 10X using a Leica DM6B Fluorescent Microscope (Leica Biosytems, Deer Park, IL, USA). The imaging settings were kept constant for all samples after determining the threshold. As a control, the second tissue section on the slide was treated with hyaluronidase and we confirmed that the hyaluronidase-treated samples did not show a positive signal and used this to help set the threshold. HABP staining intensity analysis was performed using Fiji (ImageJ). Hyaluronic acid staining is reported as a ratio of HABP intensity per area in the total ovarian section. The background was determined using the hyaluronidase-treated sections, and this value was subtracted from the hyaluronic acid positive sections.

Statistical analysis

Data were analyzed using Prism Software version 9.3.1 (GraphPad, La Jolla, CA, USA) and R version 4.4.2.

Descriptive statistics expressed as the mean ± standard error of means (SEM). Visual inspection demonstrated follicle number per area and standardized follicle number data to be skewed and contained clusters of zeros. Therefore, the original data set was log transformed. For outcomes with positive values, the natural logarithm was taken directly. For outcomes with zero values, a small constant (half of the smallest positive outcome value) was added before applying the logarithm to avoid undefined values. We used unpaired t-tests to determine significance between two groups and one-way analysis of variance (ANOVA) with a Tukey's post hoc test to determine significance between three or more groups. To evaluate the effect of two independent variables (diet and age or menstrual cyclicity) on follicle number, two-way ANOVA was used. Levene's test for homogeneity of variances was performed for all two-way ANOVA analyses; all models met the homogeneity assumption except for one (multilayer follicle number per area), which showed borderline heteroscedasticity ($p = 0.042$). Tukey's post hoc test was applied when one or both of the main effects were statistically significant. To compare the follicle distribution pie charts in Figure 4, Chi-square test was used to compare the observed distribution for each experimental group against the average distribution of young control and young calorie-restricted animals. For all statistical analyses, significance was set at unadjusted or adjusted $p < 0.05$. In all figures, data are plotted untransformed and statistical tests are performed on log transformed data. P-values for main effects and interaction testing from two-way ANOVAs are shown in Supplementary Tables 1, 3, 5, and 6. Statistically significant pairwise comparisons are shown visually in the figures with asterisks signifying level of significance.

Abbreviations

AMF: abnormal morphologic features; ANOVA: analysis of variance; CON: control (ad libitum) diet; CR: caloric restriction; DAPI: 4',6'-diamnidino-2-phenylindole; E2: estradiol; FSH: follicle-stimulating hormone; HABP: hyaluronic acid binding protein; H&E: hematoxylin and eosin; IACUC: Institutional Animal Care and Use Committee; LH: luteinizing hormone; mTOR: mammalian target of rapamycin; NHP: non-human primate; PBS: phosphate buffered saline; PSR: Picrosirius Red; P4: progesterone; SEM: standard error of means; SIRT: sirtuin.

AUTHOR CONTRIBUTIONS

FED and MZ conceptualized and supervised the study, provided funding and resources, and supported the methodology and data analysis. FED oversaw project administration. ESG, RS, RG, and CM performed the experiments and analyzed, validated, and visualized the data. ESG, JS and JL performed statistical analysis. EG, RS, FD, and MZ wrote the manuscript. All authors read and approved the final manuscript.

CONFLICTS OF INTEREST

The authors declare no conflicts of interest related to this study.

ETHICAL STATEMENT

All procedures were conducted in accordance with National Research Council's Guide for the Care and Use of Laboratory Animals and approved by the Institutional Animal Care and Use Committee (IACUC of the Oregon National Primate Research Center), Protocol # 0589-07.

REFERENCES

1. American College of Obstetricians and Gynecologists Committee on Gynecologic Practice and Practice Committee. Female age-related fertility decline. Committee Opinion No. 589. Fertil Steril. 2014; 101:633–4.

https://doi.org/10.1016/j.fertnstert.2013.12.032
PMID:24559617

2. Hansen KR, Knowlton NS, Thyer AC, Charleston JS, Soules MR, Klein NA. A new model of reproductive aging: the decline in ovarian non-growing follicle number from birth to menopause. Hum Reprod. 2008; 23:699–708.
https://doi.org/10.1093/humrep/dem408
PMID:18192670

3. Cui J, Shen Y, Li R. Estrogen synthesis and signaling pathways during aging: from periphery to brain. Trends Mol Med. 2013; 19:197–209.
https://doi.org/10.1016/j.molmed.2012.12.007
PMID:23348042

4. Amargant F, Manuel SL, Tu Q, Parkes WS, Rivas F, Zhou LT, Rowley JE, Villanueva CE, Hornick JE, Shekhawat GS, Wei JJ, Pavone ME, Hall AR, et al. Ovarian stiffness increases with age in the mammalian ovary and depends on collagen and hyaluronan matrices. Aging Cell. 2020; 19:e13259.
https://doi.org/10.1111/acel.13259
PMID:33079460

5. Ouni E, Bouzin C, Dolmans MM, Marbaix E, Pyr Dit Ruys S, Vertommen D, Amorim CA. Spatiotemporal changes in mechanical matrisome components of the human ovary from prepuberty to menopause. Hum Reprod. 2020; 35:1391–410.
https://doi.org/10.1093/humrep/deaa100
PMID:32539154

6. te Velde ER, Pearson PL. The variability of female reproductive ageing. Hum Reprod Update. 2002; 8:141–54.
https://doi.org/10.1093/humupd/8.2.141
PMID:12099629

7. Osterman MJK, Hamilton BE, Martin JA, Driscoll AK, Valenzuela CP. Births: Final Data for 2021. Natl Vital Stat Rep. 2023; 72:1–53.
PMID:36723449

8. McCay CM, Crowell MF, Maynard LA. The effect of retarded growth upon the length of life span and upon the ultimate body size. 1935. Nutrition. 1989; 5:155–71.
PMID:2520283

9. Bross TG, Rogina B, Helfand SL. Behavioral, physical, and demographic changes in Drosophila populations through dietary restriction. Aging Cell. 2005; 4:309–17.
https://doi.org/10.1111/j.1474-9726.2005.00181.x
PMID:16300483

10. Wang T, Tsui B, Kreisberg JF, Robertson NA, Gross AM, Yu MK, Carter H, Brown-Borg HM, Adams PD, Ideker T. Epigenetic aging signatures in mice livers are slowed by dwarfism, calorie restriction and rapamycin treatment. Genome Biol. 2017; 18:57.
https://doi.org/10.1186/s13059-017-1186-2
PMID:28351423

11. Harper JM, Leathers CW, Austad SN. Does caloric restriction extend life in wild mice? Aging Cell. 2006; 5:441–9.
https://doi.org/10.1111/j.1474-9726.2006.00236.x
PMID:17054664

12. Wang C, Weindruch R, Fernández JR, Coffey CS, Patel P, Allison DB. Caloric restriction and body weight independently affect longevity in Wistar rats. Int J Obes Relat Metab Disord. 2004; 28:357–62.
https://doi.org/10.1038/sj.ijo.0802518
PMID:14724654

13. Walsh ME, Shi Y, Van Remmen H. The effects of dietary restriction on oxidative stress in rodents. Free Radic Biol Med. 2014; 66:88–99.
https://doi.org/10.1016/j.freeradbiomed.2013.05.037
PMID:23743291

14. Mattison JA, Roth GS, Beasley TM, Tilmont EM, Handy AM, Herbert RL, Longo DL, Allison DB, Young JE, Bryant M, Barnard D, Ward WF, Qi W, et al. Impact of caloric restriction on health and survival in rhesus monkeys from the NIA study. Nature. 2012; 489:318–21.
https://doi.org/10.1038/nature11432
PMID:22932268

15. Colman RJ, Beasley TM, Kemnitz JW, Johnson SC, Weindruch R, Anderson RM. Caloric restriction reduces age-related and all-cause mortality in rhesus monkeys. Nat Commun. 2014; 5:3557.
https://doi.org/10.1038/ncomms4557
PMID:24691430

16. Garcia DN, Saccon TD, Pradiee J, Rincón JAA, Andrade KRS, Rovani MT, Mondadori RG, Cruz LAX, Barros CC, Masternak MM, Bartke A, Mason JB, Schneider A. Effect of caloric restriction and rapamycin on ovarian aging in mice. Geroscience. 2019; 41:395–408.
https://doi.org/10.1007/s11357-019-00087-x
PMID:31359237

17. Holehan AM, Merry BJ. The control of puberty in the dietary restricted female rat. Mech Ageing Dev. 1985; 32:179–91.
https://doi.org/10.1016/0047-6374(85)90078-8
PMID:3937000

18. Merry BJ, Holehan AM. Onset of puberty and duration of fertility in rats fed a restricted diet. J Reprod Fertil. 1979; 57:253–9.
https://doi.org/10.1530/jrf.0.0570253
PMID:513013

19. Selesniemi K, Lee HJ, Tilly JL. Moderate caloric restriction initiated in rodents during adulthood sustains function of the female reproductive axis into advanced chronological age. Aging Cell. 2008; 7:622–9. https://doi.org/10.1111/j.1474-9726.2008.00409.x PMID:18549458

20. Mattison JA, Colman RJ, Beasley TM, Allison DB, Kemnitz JW, Roth GS, Ingram DK, Weindruch R, de Cabo R, Anderson RM. Caloric restriction improves health and survival of rhesus monkeys. Nat Commun. 2017; 8:14063. https://doi.org/10.1038/ncomms14063 PMID:28094793

21. Du Y, Fan TY, Tan Y, Xiong Z, Wang Z. Seasonal changes in the reproductive physiology of female rhesus macaques (Macaca mulatta). J Am Assoc Lab Anim Sci. 2010; 49:289–93. PMID:20587158

22. Heape W. The sexual season of mammals. Q J Microsc Sci. 1900; 44:1–70. https://doi.org/10.1242/jcs.s2-44.173.1

23. Wang S, Zheng Y, Li J, Yu Y, Zhang W, Song M, Liu Z, Min Z, Hu H, Jing Y, He X, Sun L, Ma L, et al. Single-Cell Transcriptomic Atlas of Primate Ovarian Aging. Cell. 2020; 180:585–600.e19. https://doi.org/10.1016/j.cell.2020.01.009 PMID:32004457

24. Walker ML, Herndon JG. Menopause in nonhuman primates? Biol Reprod. 2008; 79:398–406. https://doi.org/10.1095/biolreprod.108.068536 PMID:18495681

25. Gilardi KV, Shideler SE, Valverde CR, Roberts JA, Lasley BL. Characterization of the onset of menopause in the rhesus macaque. Biol Reprod. 1997; 57:335–40. https://doi.org/10.1095/biolreprod57.2.335 PMID:9241047

26. Epelbaum J, Terrien J. Mini-review: Aging of the neuroendocrine system: Insights from nonhuman primate models. Prog Neuropsychopharmacol Biol Psychiatry. 2020; 100:109854. https://doi.org/10.1016/j.pnpbp.2019.109854 PMID:31891735

27. Chik CL, Almeida OF, Libré EA, Booth JD, Renquist D, Merriam GR. Photoperiod-driven changes in reproductive function in male rhesus monkeys. J Clin Endocrinol Metab. 1992; 74:1068–74. https://doi.org/10.1210/jcem.74.5.1569154 PMID:1569154

28. Beltran-Frutos E, Casarini L, Santi D, Brigante G. Seasonal reproduction and gonadal function: a focus on humans starting from animal studies. Biol Reprod. 2022; 106:47–57.

https://doi.org/10.1093/biolre/ioab199 PMID:34718419

29. Ingram DK, de Cabo R, Anson RM, Ottinger MA, Lane MA, Roth GS, Mattison JA. Calorie Restriction in Nonhuman Primates: Impact on Aging, Disease, and Frailty. Longevity and Frailty. Research and Perspectives in Longevity. Berlin, Heidelberg: Springer. 2005; 39–56. https://doi.org/10.1007/3-540-27388-3_4

30. Faddy MJ, Telfer E, Gosden RG. The kinetics of pre-antral follicle development in ovaries of CBA/Ca mice during the first 14 weeks of life. Cell Tissue Kinet. 1987; 20:551–60. https://doi.org/10.1111/j.1365-2184.1987.tb01364.x PMID:3502925

31. Mattison JA, Lane MA, Roth GS, Ingram DK. Calorie restriction in rhesus monkeys. Exp Gerontol. 2003; 38:35–46. https://doi.org/10.1016/s0531-5565(02)00146-8 PMID:12543259

32. Ingram DK, Cutler RG, Weindruch R, Renquist DM, Knapka JJ, April M, Belcher CT, Clark MA, Hatcherson CD, Marriott BM, Roth GS. Dietary restriction and aging: the initiation of a primate study. J Gerontol. 1990; 45:B148–63. https://doi.org/10.1093/geronj/45.5.b148 PMID:2394908

33. Acosta-Rodríguez V, Rijo-Ferreira F, Izumo M, Xu P, Wight-Carter M, Green CB, Takahashi JS. Circadian alignment of early onset caloric restriction promotes longevity in male C57BL/6J mice. Science. 2022; 376:1192–202. https://doi.org/10.1126/science.abk0297 PMID:35511946

34. Ferreira ARO, Ribeiro MVG, Peres MNC, Piovan S, Gonçalves GD, Saavedra LPJ, Martins JNL, Junior MDF, Cavalcante KVN, Lopes GKG, Carneiro M, Almeida DL, Gomes RM, et al. Protein Restriction in the Peri-Pubertal Period Induces Autonomic Dysfunction and Cardiac and Vascular Structural Changes in Adult Rats. Front Physiol. 2022; 13:840179. https://doi.org/10.3389/fphys.2022.840179 PMID:35574445

35. Rizzoto G, Sekhar D, Thundathil JC, Chelikani PK, Kastelic JP. Calorie Restriction Modulates Reproductive Development and Energy Balance in Pre-Pubertal Male Rats. Nutrients. 2019; 11:1993. https://doi.org/10.3390/nu11091993 PMID:31450760

36. Briley SM, Jasti S, McCracken JM, Hornick JE, Fegley B, Pritchard MT, Duncan FE. Reproductive age-associated fibrosis in the stroma of the mammalian ovary. Reproduction. 2016; 152:245–60.

https://doi.org/10.1530/REP-16-0129
PMID:27491879

37. Ouni E, Peaucelle A, Haas KT, Van Kerk O, Dolmans MM, Tuuri T, Otala M, Amorim CA. A blueprint of the topology and mechanics of the human ovary for next-generation bioengineering and diagnosis. Nat Commun. 2021; 12:5603.
https://doi.org/10.1038/s41467-021-25934-4
PMID:34556652

38. Amargant F, Manuel SL, Larmore MJ, Johnson BW, Lawson M, Pritchard MT, Zelinski MB, Duncan FE. Sphingosine-1-phosphate and its mimetic FTY720 do not protect against radiation-induced ovarian fibrosis in the nonhuman primate†. Biol Reprod. 2021; 104:1058–70.
https://doi.org/10.1093/biolre/ioab012
PMID:33524104

39. Rowley JE, Rubenstein GE, Manuel SL, Johnson NL, Surgnier J, Kapitsinou PP, Duncan FE, Pritchard MT. Tissue-specific Fixation Methods Are Required for Optimal In Situ Visualization of Hyaluronan in the Ovary, Kidney, and Liver. J Histochem Cytochem. 2020; 68:75–91.
https://doi.org/10.1369/0022155419884879
PMID:31714169

40. McShane TM, Wise PM. Life-long moderate caloric restriction prolongs reproductive life span in rats without interrupting estrous cyclicity: effects on the gonadotropin-releasing hormone/luteinizing hormone axis. Biol Reprod. 1996; 54:70–5.
https://doi.org/10.1095/biolreprod54.1.70
PMID:8838002

41. Dirks AJ, Leeuwenburgh C. Caloric restriction in humans: potential pitfalls and health concerns. Mech Ageing Dev. 2006; 127:1–7.
https://doi.org/10.1016/j.mad.2005.09.001
PMID:16226298

42. Li PL, Huang CH, Mao L, Li J, Sheng ZG, Zhu BZ. An unprecedented free radical mechanism for the formation of DNA adducts by the carcinogenic N-sulfonated metabolite of aristolochic acids. Free Radic Biol Med. 2023; 205:332–45.
https://doi.org/10.1016/j.freeradbiomed.2023.05.005
PMID:37179032

43. Lujan ME, Krzemien AA, Reid RL, Van Vugt DA. Caloric restriction inhibits steroid-induced gonadotropin surges in ovariectomized rhesus monkeys. Endocrine. 2005; 27:25–31.
https://doi.org/10.1385/ENDO:27:1:025
PMID:16077167

44. López-Otín C, Blasco MA, Partridge L, Serrano M, Kroemer G. The hallmarks of aging. Cell. 2013; 153:1194–217.

https://doi.org/10.1016/j.cell.2013.05.039
PMID:23746838

45. Yu BP, Chung HY. Stress resistance by caloric restriction for longevity. Ann N Y Acad Sci. 2001; 928:39–47.
https://doi.org/10.1111/j.1749-6632.2001.tb05633.x
PMID:11795526

46. Long GY, Yang JY, Xu JJ, Ni YH, Zhou XL, Ma JY, Fu YC, Luo LL. SIRT1 knock-in mice preserve ovarian reserve resembling caloric restriction. Gene. 2019; 686:194–202.
https://doi.org/10.1016/j.gene.2018.10.040
PMID:30340050

47. Dou X, Sun Y, Li J, Zhang J, Hao D, Liu W, Wu R, Kong F, Peng X, Li J. Short-term rapamycin treatment increases ovarian lifespan in young and middle-aged female mice. Aging Cell. 2017; 16:825–36.
https://doi.org/10.1111/acel.12617
PMID:28544226

48. Arslan NP, Taskin M, Keles ON. Nicotinamide Mononucleotide and Nicotinamide Riboside Reverse Ovarian Aging in Rats Via Rebalancing Mitochondrial Fission and Fusion Mechanisms. Pharm Res. 2024; 41:921–35.
https://doi.org/10.1007/s11095-024-03704-3
PMID:38684562

49. McCloskey CW, Cook DP, Kelly BS, Azzi F, Allen CH, Forsyth A, Upham J, Rayner KJ, Gray DA, Boyd RW, Murugkar S, Lo B, Trudel D, et al. Metformin Abrogates Age-Associated Ovarian Fibrosis. Clin Cancer Res. 2020; 26:632–42.
https://doi.org/10.1158/1078-0432.CCR-19-0603
PMID:31597663

50. Qin X, Du D, Chen Q, Wu M, Wu T, Wen J, Jin Y, Zhang J, Wang S. Metformin prevents murine ovarian aging. Aging (Albany NY). 2019; 11:3785–94.
https://doi.org/10.18632/aging.102016
PMID:31182682

51. Umehara T, Winstanley YE, Andreas E, Morimoto A, Williams EJ, Smith KM, Carroll J, Febbraio MA, Shimada M, Russell DL, Robker RL. Female reproductive life span is extended by targeted removal of fibrotic collagen from the mouse ovary. Sci Adv. 2022; 8:eabn4564.
https://doi.org/10.1126/sciadv.abn4564
PMID:35714185

52. Tilly JL. Ovarian follicle counts--not as simple as 1, 2, 3. Reprod Biol Endocrinol. 2003; 1:11.
https://doi.org/10.1186/1477-7827-1-11
PMID:12646064

53. National Research Council (US) Committee for the Update of the Guide for the Care and Use of

Laboratory Animals. Guide for the Care and Use of Laboratory Animals. 8th ed. Washington (DC): National Academies Press (US). 2011.
https://doi.org/10.17226/12910
PMID:21595115

54. Downs JL, Mattison JA, Ingram DK, Urbanski HF. Effect of age and caloric restriction on circadian adrenal steroid rhythms in rhesus macaques. Neurobiol Aging. 2008; 29:1412–22.
https://doi.org/10.1016/j.neurobiolaging.2007.03.011
PMID:17420071

55. Sitzmann BD, Leone EH, Mattison JA, Ingram DK, Roth GS, Urbanski HF, Zelinski MB, Ottinger MA. Effects of moderate calorie restriction on testosterone production and semen characteristics in young rhesus macaques (Macaca mulatta). Biol Reprod. 2010; 83:635–40.
https://doi.org/10.1095/biolreprod.110.084186
PMID:20610809

56. Black A, Allison DB, Shapses SA, Tilmont EM, Handy AM, Ingram DK, Roth GS, Lane MA. Calorie restriction and skeletal mass in rhesus monkeys (Macaca mulatta): evidence for an effect mediated through changes in body size. J Gerontol A Biol Sci Med Sci. 2001; 56:B98–107.
https://doi.org/10.1093/gerona/56.3.b98
PMID:11253152

57. Mattison JA, Black A, Huck J, Moscrip T, Handy A, Tilmont E, Roth GS, Lane MA, Ingram DK. Age-related decline in caloric intake and motivation for food in rhesus monkeys. Neurobiol Aging. 2005; 26:1117–27.
https://doi.org/10.1016/j.neurobiolaging.2004.09.013
PMID:15748792

58. Koering MJ. Preantral follicle development during the menstrual cycle in the Macaca mulatta ovary. Am J Anat. 1983; 166:429–43.
https://doi.org/10.1002/aja.1001660405
PMID:6858940

59. O'Neill KE, Maher JY, Laronda MM, Duncan FE, LeDuc RD, Lujan ME, Oktay KH, Pouch AM, Segars JH, Tsui EL, Zelinski MB, Halvorson LM, Gomez-Lobo V. Anatomic nomenclature and 3-dimensional regional model of the human ovary: call for a new paradigm. Am J Obstet Gynecol. 2023; 228:270–5.e4.
https://doi.org/10.1016/j.ajog.2022.09.040
PMID:36191605

60. Mara JN, Zhou LT, Larmore M, Johnson B, Ayiku R, Amargant F, Pritchard MT, Duncan FE. Ovulation and ovarian wound healing are impaired with advanced reproductive age. Aging (Albany NY). 2020; 12:9686–713.
https://doi.org/10.18632/aging.103237
PMID:32407290
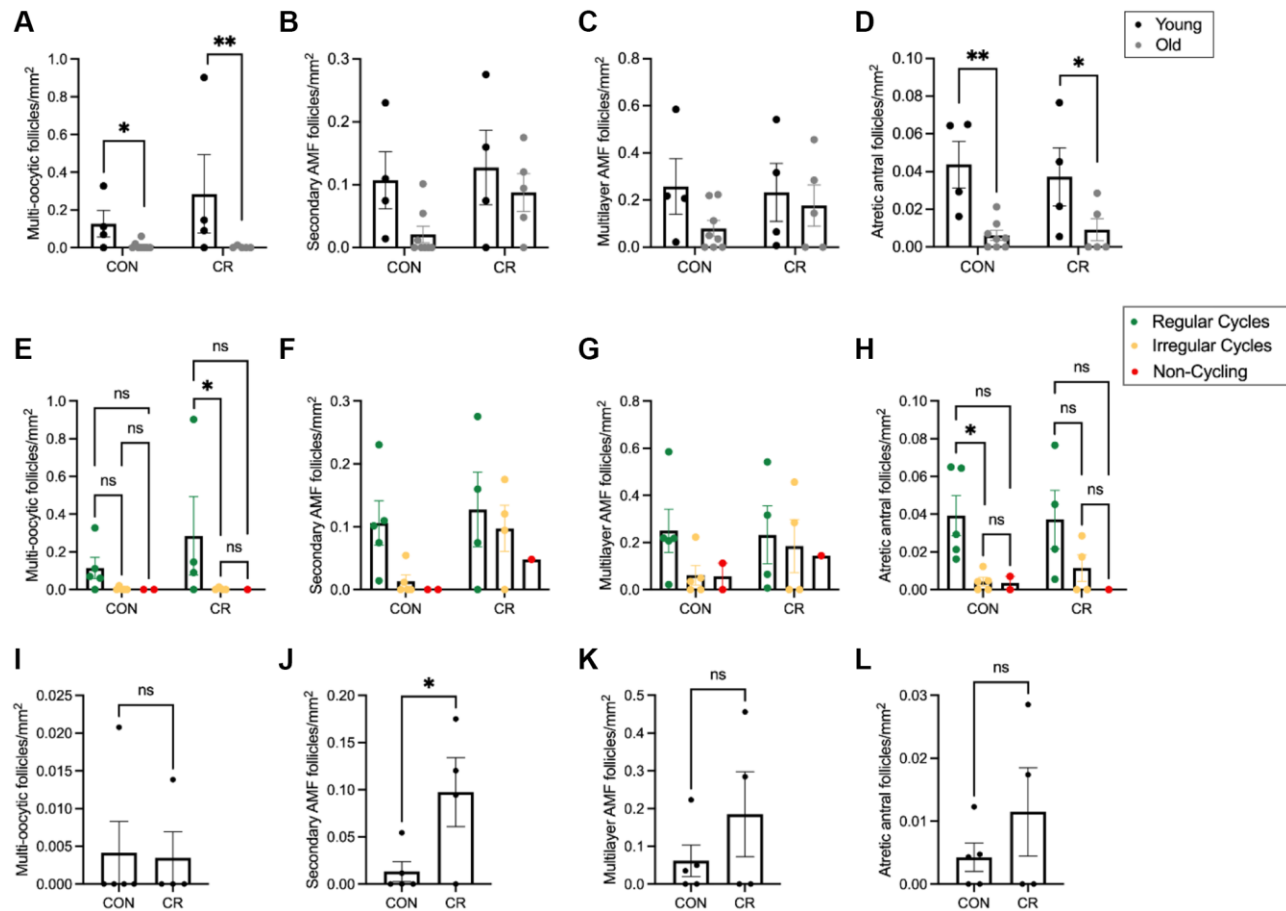
Supplementary Figure 1. Follicle number for abnormal follicle morphologies per ovarian section area. Bar graphs comparing the effect of age and diet on follicle number per ovarian section area are shown for each abnormal follicle morphology class including: (**A**) multi-oocytic, (**B**) secondary with abnormal morphologic features (AMF), (**C**) multilayer with AMF, and (**D**) atretic antral follicles. Bar graphs comparing the effect of reproductive status and diet on follicle number per ovarian section area for each abnormal follicle morphology class including: (**E**) multi-oocytic, (**F**) secondary with AMF, (**G**) multilayer with AMF, and (**H**) atretic antral follicles. Bar graphs comparing the effect of diet on follicle number per ovarian section area for each abnormal follicle morphology class are shown in old animals with irregular cycles including: (**I**) multi-oocytic, (**J**) secondary with AMF, (**K**) multilayer with AMF, and (**L**) atretic antral follicles. Data are presented as mean ± SEM. In (**A–D**), black circles represent young animals and gray circles represent old animals. In (**E–H**), green circles represent animals with regular cycles, yellow circles represent animals with irregular cycles, and red circles represent non-cycling animals. Untransformed data are plotted. Statistics were calculated using a two-way ANOVA with Tukey's multiple comparison test (if appropriate) on log-transformed data for (**A–H**) and an unpaired *t*-test on untransformed data (**I–L**). *P*-values for sources of variation of two-way ANOVA can be found in Supplementary Tables 1 and 5. $^{*}p \leq 0.05$ and $^{**}p \leq 0.01$.
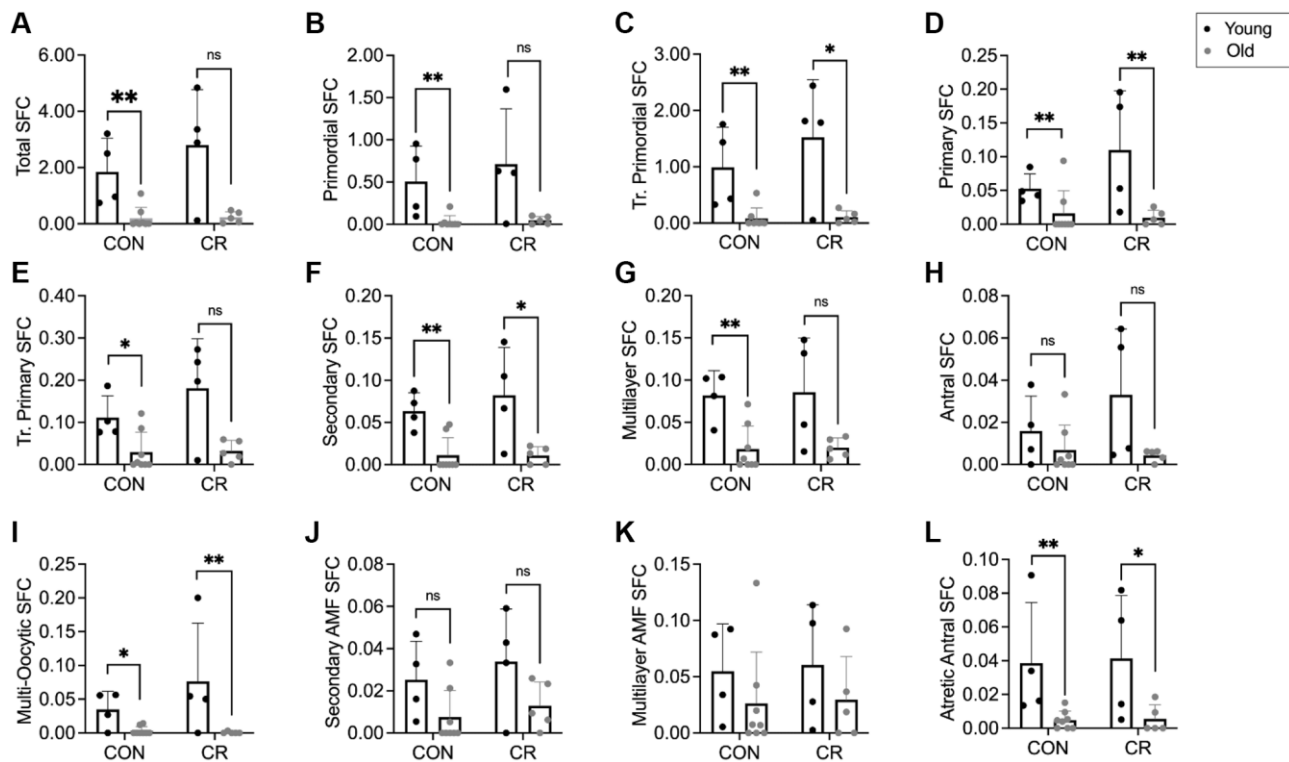
Supplementary Figure 2. Standardized follicle number as a function of age and diet. Standardized follicle number was calculated by summing the follicle number per class in each individual animal and dividing by the number of histologic slides generated for that animal. Bar graphs highlighting standardized follicle number for each normal and abnormal follicle morphology class are shown including: (**A**) total number of follicles, (**B**) primordial, (**C**) transitional primordial, (**D**) primary, (**E**) transitional primary, (**F**) secondary, (**G**) multilayer, (**H**) antral, (**I**) multi-oocytic, (**J**) secondary with abnormal morphologic features (AMF) (**K**) multilayer with AMF, and (**L**) atretic antral follicles. Data are presented as mean ± SEM. Black circles indicate young animals and grey circles indicate old animals. Untransformed data are plotted. Statistics were calculated using a two-way ANOVA with Tukey's multiple comparison test (if appropriate) on log-transformed data. *P*-values for sources of variation of two-way ANOVA can be found in Supplementary Table 3. $^*p \leq 0.05$, $^{**}p \leq 0.01$.
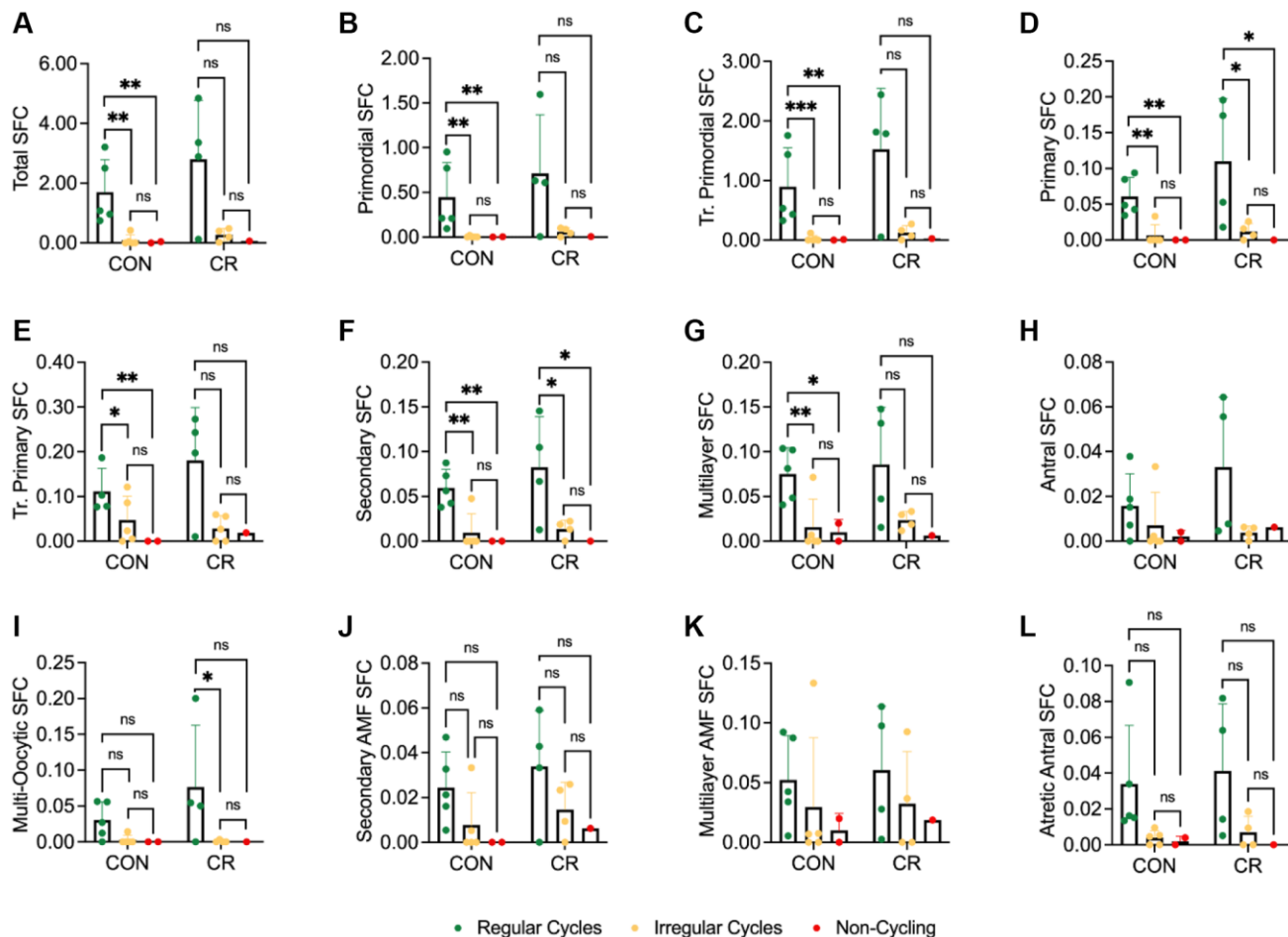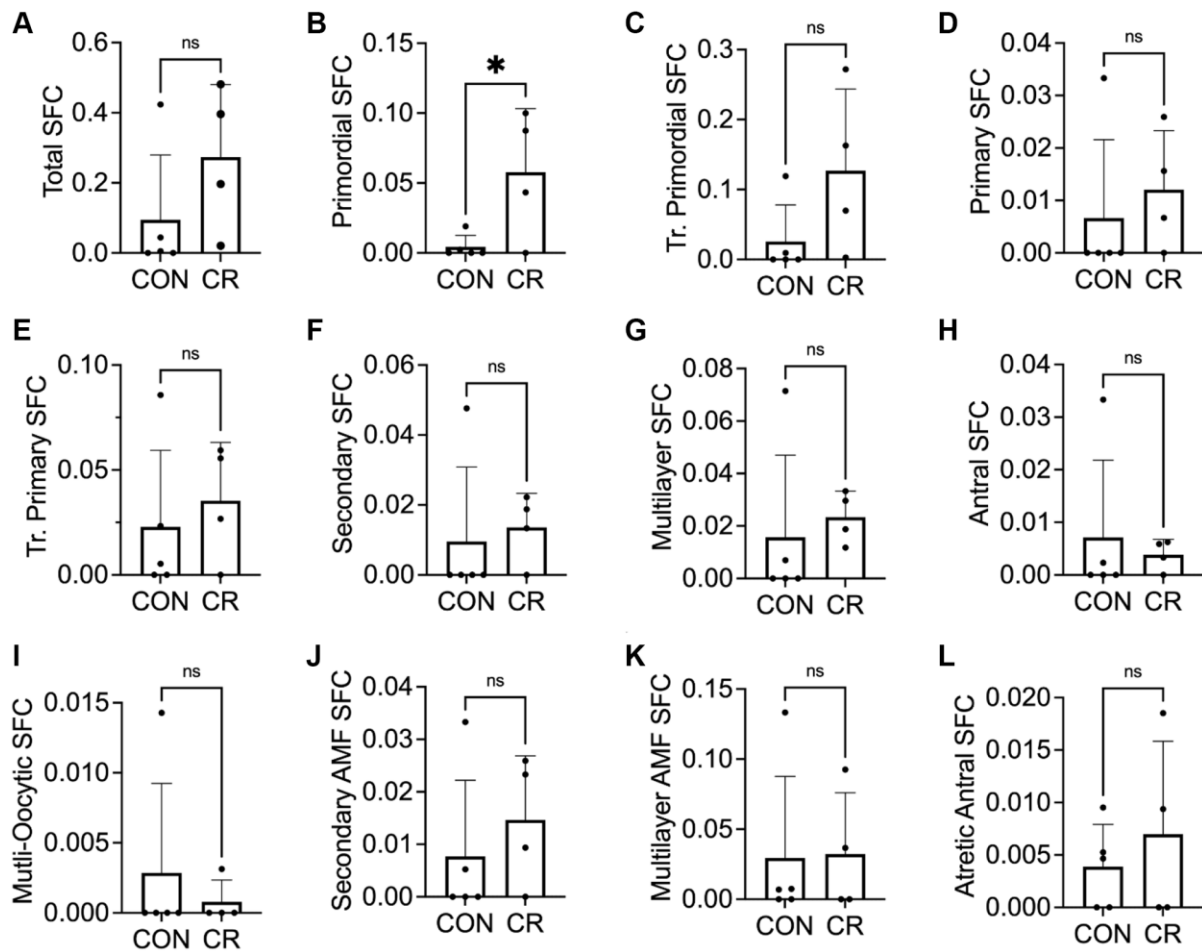
Supplementary Figure 3. Standardized follicle number as a function of reproductive status and diet. Standardized follicle number was calculated by summing the follicle number per class in each individual animal and dividing by the number of histologic slides generated for that animal. Bar graphs highlighting standardized follicle count for each normal and abnormal follicle morphology class are shown including: (**A**) total number of follicles, (**B**) primordial, (**C**) transitional primordial, (**D**) primary, (**E**) transitional primary, (**F**) secondary, (**G**) multilayer, (**H**) antral, (**I**) multi-oocytic, (**J**) secondary with abnormal morphologic features (AMF) (**K**) multilayer with AMF, and (**L**) atretic antral follicles. Data are presented as mean ± SEM. Green circles represent animals with regular cycles, yellow circles represent animals with irregular cycles, and red circles represent non-cycling animals. Untransformed data are plotted. Statistics were calculated with a two-way ANOVA with Tukey's multiple comparison test (if appropriate) on log-transformed data. *$p \leq 0.05$, **$p \leq 0.01$, ***$p \leq 0.001$. *P*-values for sources of variation of two-way ANOVA can be found in Supplementary Table 5.

Supplementary Figure 4. Standardized follicle number as a function of diet in old animals with irregular cycles. Standardized follicle number was calculated by summing the follicle number per class in each individual animal and dividing by the number of histologic slides generated for that animal. Bar graphs highlighting standardized follicle number for each follicle morphology class are shown including: (**A**) total number of follicles, (**B**) primordial, (**C**) transitional primordial, (**D**) primary, (**E**) transitional primary, (**F**) secondary, (**G**) multilayer, (**H**) antral, (**I**) multi-oocytic, (**J**) secondary with abnormal morphologic features (AMF) (**K**) multilayer with AMF, and (**L**) atretic antral follicles. Data are presented as mean ± SEM. Statistics were calculated using an unpaired *t*-test. *$p \leq 0.05$.

Supplementary Tables

Supplementary Table 1. Statistical analysis of homogeneity of variation, sources of variation and main effects for follicle number per area as a function of diet and age.

Follicle Class	Levene's test for homogeneity of variance	Source of variation		
		Interaction	Diet	Age
Total	ns: $p = 0.1451$	ns: $p = 0.1815$	ns: $p = 0.1667$	$^{**}p = 0.0010$
Primordial	ns: $p = 0.9574$	ns: $p = 0.1592$	ns: $p = 0.2856$	$^{***}p = 0.0009$
Tr. Primordial	ns: $p = 0.639$	ns: $p = 0.2391$	ns: $p = 0.2145$	$^{***}p = 0.00005$
Primary	ns: $p = 0.7207$	ns: $p = 0.7258$	ns: $p = 0.4527$	$^{***}p = 0.0007$
Tr. Primary	ns: $p = 0.6891$	ns: $p = 0.4048$	ns: $p = 0.4350$	$^{**}p = 0.0090$
Secondary	ns: $p = 0.8815$	ns: $p = 0.2913$	ns: $p = 0.4619$	$^{***}p = 0.0003$
Multilayer	$^{*}0.0416$	ns: $p = 0.1736$	ns: $p = 0.4053$	$^{**}p = 0.0077$
Antral	ns: $p = 0.8419$	ns: $p = 0.9163$	ns: $p = 0.2701$	ns: $p = 0.0726$
Multi-oocytic	ns: $p = 0.2819$	ns: $p = 0.5965$	ns: $p = 0.9949$	$^{**}p = 0.0017$
Secondary with AMF	ns: $p = 0.9453$	ns: $p = 0.1755$	ns: $p = 0.1633$	ns: $p = 0.0654$
Multilayer with AMF	ns: $p = 0.6337$	ns: $p = 0.6040$	ns: $p = 0.8870$	ns: $p = 0.1440$
Atretic Antral	ns: 0.8485	ns: $p = 0.7445$	ns: $p = 0.7463$	$^{**}p = 0.0012$

Supplementary Table 2. Animal characteristics, including age at necropsy, cyclicity, and ovary weight for each individual animal in the study.

	Animal ID	Group	Age at necropsy (yrs)	Cyclicity	Ovary weight (mg)
Y-CON-1	22360	Young, Control	10	Regular	326
Y-CON-2	22362	Young, Control	13	Regular	578
Y-CON-3	22365	Young, Control	13	Regular	314
Y-CON-4	22367	Young, Control	13	Regular	314
O-CON-1	22342	Old, Control	26	Non-cycling	151
O-CON-2	22343	Old, Control	22	Irregular	377
O-CON-3	22345	Old, Control	26	Non-cycling	155
O-CON-4	22350	Old, Control	22	Irregular	200
O-CON-5	22351	Old, Control	22	Irregular	255
O-CON-6	22352	Old, Control	19	Regular	326
O-CON-7	22355	Old, Control	25	Irregular	340
O-CON-8	22368	Old, Control	25	Irregular	145
Y-CR-1	22357	Young, CR	13	Regular	400
Y-CR-2	22359	Young, CR	13	Regular	205
Y-CR-3	22361	Young, CR	13	Regular	360
Y-CR-4	22364	Young, CR	13	Regular	554
O-CR-1	22341	Old, CR	26	Irregular	226
O-CR-2	22347	Old, CR	25	Non-cycling	72
O-CR-3	22353	Old, CR	21	Irregular	210
O-CR-4	22354	Old, CR	20	Irregular	165
O-CR-5	22356	Old, CR	23	Irregular	125

Supplementary Table 3. Statistical analysis of homogeneity of variation, sources of variation and main effects for standardized follicle count (SFC) as a function of diet and age.

Follicle Class	Levene's test for homogeneity of variance	Source of variation		
		Interaction	Diet	Age
Total	ns: $p = 0.1621$	ns: $p = 0.3015$	ns: $p = 0.2005$	***$p = 0.0005$
Primordial	ns: $p = 0.9553$	ns: $p = 0.2947$	ns: $p = 0.3586$	***$p = 0.0006$
Tr. Primordial	ns: $p = 0.5130$	ns: $p = 0.3298$	ns: $p = 0.2103$	***$p = 0.0003$
Primary	ns: $p = 0.7806$	ns: $p = 0.8938$	ns: $p = 0.5039$	***$p = 0.0004$
Tr. Primary	ns: $p = 0.4447$	ns: $p = 0.5693$	ns: $p = 0.4096$	**$p = 0.0039$
Secondary	ns: $p = 0.8815$	ns: $p = 0.7486$	ns: $p = 0.6251$	***$p = 0.0002$
Multilayer	ns: $p = 0.1038$	ns: $p = 0.3257$	ns: $p = 0.4218$	**$p = 0.0015$
Antral	ns: $p = 0.5314$	ns: $p = 0.6601$	ns: $p = 0.3867$	*$p = 0.0352$
Multi-oocytic	ns: $p = 0.5401$	ns: $p = 0.5215$	ns: $p = 0.9632$	**$p = 0.0012$
Secondary with AMF	ns: $p = 0.9874$	ns: $p = 0.4689$	ns: $p = 0.3682$	*$p = 0.0353$
Multilayer with AMF	ns: $p = 0.7935$	ns: $p = 0.8251$	ns: $p = 0.8936$	ns: p = 0.0896
Atretic Antral	ns: $p = 0.8685$	ns: $p = 0.9752$	ns: $p = 0.7993$	***$p = 0.0007$

Supplementary Table 4. Raw follicle number data (mean/median/min/max) for young control, young calorie-restricted (CR), old control, and old calorie-restricted (CR) for all follicle classes (normal and abnormal).

		Primordial	Tr. Primordial	Primary	Tr. Primary	Secondary	Multilayer	Antral	Total	Secondary AMF	Multilayer AMF	Atretic Antral	Multi-oocytic
Young CON	Mean	232	448	24.3	50.8	29.8	38	6	828.8	14.3	10.8	24.3	15.3
	Median	201.5	387	21	40.5	28	39.5	5	727	14	12	23.5	13
	Min.	30	105	11	25	14	15	0	221	0	2	2	6
	Max.	495	913	44	97	49	58	14	1640	29	17	48	29
Young CR	Mean	209	490.8	35.5	59.3	26.3	28.5	12.8	862	28.5	10.8	19.3	12.3
	Median	241.5	590	31	65.5	28	23	11.5	1037	15	12.5	17.5	12
	Min.	2	21	7	4	5	6	1	48	0	0	1	2
	Max.	351	762	73	102	44	62	27	1326	84	18	41	23
Old CON	Mean	9.4	26	4.8	8.7	3	4.9	1.8	58.4	0.875	1.875	6.5	1.8
	Median	0.5	1.5	0	0.5	0	1.5	0.5	5.5	0	0	2.5	1
	Min.	0	0	0	0	0	0	0	0	0	0	0	0
	Max.	69	176	31	40	14	16	7	351	4	7	28	5
Old CR	Mean	13.8	31.4	2.8	9	3.2	5.8	1.2	67.2	0.2	3.6	7.8	1.6
	Median	13	21	2	8	4	6	1	59	0	3	3	0
	Min.	0	1	0	0	0	1	0	7	0	0	0	0
	Max.	28	87	7	19	6	10	2	153	1	7	25	5

Supplementary Table 5. Statistical analysis of homogeneity of variation, sources of variation and main effects for follicle number per area as a function of diet and menstrual cyclicity.

Follicle class	Levene's test for homogeneity of variance	Source of variation		
		Interaction	Diet	Menstrual cyclicity
Total	ns: $p = 0.6020$	ns: $p = 0.1831$	ns: $p = 0.708$	***$p = 0.0007$
Primordial	ns: $p = 0.8660$	ns: $p = 0.1527$	ns: $p = 0.1339$	***$p = 0.0006$
Tr. Primordial	ns: $p = 0.9522$	ns: $p = 0.2370$	ns: $p = 0.0864$	***$p = 0.0003$
Primary	ns: $p = 0.1314$	ns: $p = 0.4250$	ns: $p = 0.2130$	***$p = 0.0001$
Tr. Primary	ns: $p = 0.6412$	ns: $p = 0.4304$	ns: $p = 0.3076$	**$p = 0.0047$
Secondary	ns: $p = 0.7078$	ns: $p = 0.2215$	ns: $p = 0.2396$	***$p = 0.0001$
Multilayer	ns: $p = 0.5879$	ns: $p = 0.1286$	ns: $p = 0.2682$	**$p = 0.0088$
Antral	ns: $p = 0.9515$	ns: $p = 0.9224$	ns: $p = 0.2219$	ns: $p = 0.976$
Multi-oocytic	ns: $p = 0.3765$	ns: $p = 0.9427$	ns: $p = 0.7696$	**$p = 0.0033$
Secondary with AMF	ns: $p = 0.7987$	ns: $p = 0.2253$	ns: $p = 0.1245$	ns: $p = 0.691$
Multilayer with AMF	ns: $p = 0.1052$	ns: $p = 0.6450$	ns: $p = 0.7790$	ns: $p = 0.2250$
Atretic Antral	ns: $p = 0.1153$	ns: $p = 0.6691$	ns: $p = 0.9526$	**$p = 0.0021$

Supplementary Table 6. Statistical analysis of homogeneity of variation, sources of variation and main effects for standardized follicle count (SFC) as a function of diet and menstrual cyclicity.

Follicle class	Levene's test for homogeneity of variance	Source of variation		
		Interaction	Diet	Menstrual cyclicity
Total	ns: $p = 0.6020$	ns: $p = 0.1831$	ns: $p = 0.708$	***$p = 0.0007$
Primordial	ns: $p = 0.8660$	ns: $p = 0.1527$	ns: $p = 0.1339$	***$p = 0.0006$
Tr. Primordial	ns: $p = 0.9522$	ns: $p = 0.2370$	ns: $p = 0.0864$	***$p = 0.0003$
Primary	ns: $p = 0.1314$	ns: $p = 0.4250$	ns: $p = 0.2130$	***$p = 0.0001$
Tr. Primary	ns: $p = 0.6412$	ns: $p = 0.4304$	ns: $p = 0.3076$	**$p = 0.0047$
Secondary	ns: $p = 0.7078$	ns: $p = 0.2215$	ns: $p = 0.2396$	***$p = 0.0001$
Multilayer	ns: $p = 0.5879$	ns: $p = 0.1286$	ns: $p = 0.2682$	**$p = 0.0088$
Antral	ns: $p = 0.9515$	ns: $p = 0.9224$	ns: $p = 0.2219$	ns: $p = 0.976$
Multi-oocytic	ns: $p = 0.3765$	ns: $p = 0.9427$	ns: $p = 0.7696$	**$p = 0.0033$
Secondary with AMF	ns: $p = 0.7987$	ns: $p = 0.2253$	ns: $p = 0.1245$	ns: $p = 0.691$
Multilayer with AMF	ns: $p = 0.1052$	ns: $p = 0.6450$	ns: $p = 0.7790$	ns: $p = 0.2250$
Atretic Antral	ns: $p = 0.1153$	ns: $p = 0.6691$	ns: $p = 0.9526$	**$p = 0.0021$